Noradrenergic *locus coeruleus* activity functionally partitions NREM sleep to gatekeep the NREM-REM sleep cycle

Alejandro Osorio-Forero[1,2], Georgios Foustoukos[1], Romain Cardis[1], Najma Cherrad, Christiane Devenoges, Laura M.J. Fernandez and Anita Lüthi

Department of Fundamental Neurosciences, University of Lausanne, Rue du Bugnon 9, CH-1005 Lausanne, Switzerland

[1] Equal contribution

[2] Department of Sleep and Cognition. Netherlands Institute for Neuroscience, Meibergdreef 47, 1105 BA Amsterdam, The Netherlands

Correspondence: anita.luthi@unil.ch

Author contributions: AOF, RC, NC, LF and AL originally started this project. GF developed all LC fiber photometry experimentation and corresponding analyses. RC developed the REMS restriction procedure. AOF and GF developed analysis scripts, and all authors contributed to data analysis. LF made the final figure versions and schemes. AL wrote the manuscript, with input from all authors.

Acknowledgements: The authors acknowledge fruitful discussions with Paul Franken, Stephany Fulda, Caroline Lustenberger, Markus Schmidt, Francesca Siclari, Aurélie Stephan, Mehdi Tafti and Eus van Someren. We thank Dr. Simone Astori and Olivia Zanoletti from the Carmen Sandi lab (EPFL, Lausanne) for carrying out the corticosterone measurements and Aurélie Guillaume-Gentil for assistance with viral injections. We recognize Dr. Sandro Lecci for providing the first datasets relevant for this study. Many thanks to Drs. Feng and Li for generously providing us with the first aliquots of the $GRAB_{NE}$ sensor. The constructive comments of Dr. Julie Buron, Lila Banterle and Paola Milanese on the manuscript are very appreciated. We are grateful to the animal caretakers, especially Michelle Blom and Titouan Tromme, and to Dr. Laure Sériot for expert veterinary advice. This work was supported by the Swiss National Science Foundation (Grant no. 184759 to AL), a FBM UNIL Doctoral Fellowship to AOF, and Etat de Vaud.

Conflict of interest. The authors declare no conflict of interest.

Abstract

The noradrenergic *locus coeruleus* (LC) is vital for brain states underlying wakefulness, whereas its roles for sleep remain uncertain. Combining mouse sleep-wake monitoring, behavioral manipulations, LC fiber photometry and closed-loop optogenetics, we found that LC neuronal activity partitioned non-rapid-eye-movement sleep (NREMS) into alternating brain and autonomic states that rule the NREMS-REMS cycle. High LC activity levels generated an autonomic-subcortical arousal state that facilitated cortical microarousals, while low levels were obligatory for REMS entries. Timed optogenetic LC inhibition revealed that this functional alternation set the duration of the NREMS-REMS cycle by ruling REMS entries during undisturbed sleep and when pressure for REMS was high. A stimulus-enriched, stress-promoting wakefulness increased high LC activity levels at the expense of low ones in subsequent NREMS, fragmenting NREMS through microarousals and delaying REMS onset. We conclude that LC activity fluctuations gatekeep the NREM-REMS cycle over recurrent infraslow intervals, but they also convey vulnerability to adverse wake experiences.

Key words: ultradian sleep cycle || arousability || sleep homeostasis || REMS restriction || automated REMS deprivation || microarousal || noradrenaline || norepinephrine || infra-slow time scale || optogenetics || K-complex || sleep disorders

Introduction

The pontine brainstem *locus coeruleus* (LC) is a wake-promoting brain area that constitutes the principal source of noradrenaline (NA) for forebrain circuits and alertness-modulating nuclei[1]. LC neuronal activity levels grade with the level of wakefulness[2] and with physiological signatures of cortical[3] and autonomic arousal[4,5], while sleep-promoting brain areas are inhibited[6,7]. Elevated LC activity is implicated in the cognitive and autonomic manifestations of states of hyperarousal during stress- and anxiety-provoking experiences[1,8]. Conversely, clinically important sedatives inhibit LC[9]. Together, this illustrates LC's broad implication in regulating arousal levels in states of wakefulness.

Many noradrenergic LC neurons remain active in sleep[7,10-14], during which they increase arousability[15,16], in line with LC's wake-promoting actions[1,3]. During non-rapid-eye-movement sleep (NREMS) in mouse, activity levels of LC neuron populations fluctuate on an infraslow time scale (30 – 50 s, 0.02 Hz), generating varying levels of free NA in the forebrain[17-19]. For example, in thalamus, NA fluctuations recurrently depolarize thalamocortical and thalamic reticular neurons. This depolarization suppresses the capacity of thalamic circuits to generate sleep spindles, known as NREMS EEG hallmarks in the 10 – 15 Hz frequency range[17] that shield NREMS from sensory disruption[20]. The LC-induced thalamic activation hence promotes auditory and somatosensory arousability[16,21,22]. Spontaneous microarousals (MAs) that are typical for mammalian NREMS also coincide preferentially with moments of low spindle density[18,21]. When reaching high levels, LC activity fluctuations generate brain states with high arousability, suggesting that they could be primarily sleep-disruptive. Alternatively, its activity fluctuations could have a broader relevance for the dynamics of sleep. For example, for sleep to take its natural progression across NREMS and REMS, it is necessary that global brain states be driven across transitory, less stable periods. In human sleep, signatures of sleep 'instability' and elevated arousability have been described[23], yet neither the underlying neural mechanisms driving these nor the associated brain states are known.

A low level of LC unit activity has further been associated with REMS[10-12]. This prompted the first circuit-based theoretical models for the mammalian NREM-REM sleep cycle, in which the LC was integrated as a REM-off area[24,25]. Indeed, optogenetic activation of NA-synthetizing LC neurons can increase the time spent in NREMS at the expense of REMS, whereas inhibition can have opposite effects[15,17-19]. Also, widely used sedatives that interfere with NA signaling modify REMS in humans[26,27]. Furthermore, the level of LC activity in wakefulness negatively associated with human REMS quality[28]. Therefore, a balanced assessment of LC actions REMS-regulatory and REMS-disruptive actions is desirable and is indeed pressing as its implication in human sleep becomes increasingly recognized[29,30].

Here, we show that LC rules the time scales over which the NREMS-REMS cycle evolves, setting the moments when transitions between NREMS and REMS are allowed, and when not. This ruling was enabled through the alternation of LC activity fluctuations between high and low levels that induced distinct brain states characterized by a unique profile of autonomic, subcortical and cortical arousal levels. High levels of LC activity fluctuations preferentially lead to MAs but suppressed REMS entries. REMS entries took place once LC activity decayed to low levels, either spontaneously or through optogenetic inhibition. We further found that the infraslow temporal alternation between high and low LC activity levels regulated the duration of the NREMS-REMS cycle and restrained it to a minimum of ~50 s during REMS restriction (REMS-R). After a stimulus-enriched wake experience, LC activity fluctuations became unbalanced and persisted at high levels, which caused more arousals and delayed REMS. The LC is hence a neural mechanism that gatekeeps the NREMS-REMS-cycle duration, but that can generate cycle disruptions as a result of preceding wake experience.

Results

High LC activity levels during NREMS promoted brain and autonomic activation that facilitates arousability

To monitor the activity of LC neurons during unperturbed sleep, we conditionally expressed the genetically encoded Ca^{2+} sensor jGCaMP8s in dopamine-β-hydroxylase-(DBH)-Cre mice, previously shown to drive the expression of viral constructs in NA-synthetizing neurons with a high degree of specificity (> 80 %, see also **Extended Data Fig. 1a**)[17,31]. We then implanted animals with EEG/EMG electrodes together with an optic fiber stub over the LC for combined sleep and fiber photometric recordings of LC neuronal activity (**Fig. 1a**, **b**). Local field potential (LFP) electrodes were additionally implanted in the primary somatosensory S1 cortex and the hippocampal CA1 area. The EEG signals served to score the major vigilance states Wake, NREMS and REMS and the MAs based on standard polysomnography[17,21,22,32]. The S1 LFP recordings were used to monitor the local thalamocortical dynamics of power bands characteristic for NREMS and the CA1 LFP recordings to define the onset of REMS (see Methods).

Across the 12-h light phase (ZT0-ZT12), the major resting phase of mice, the photometrically recorded Ca^{2+} activity of noradrenergic LC populations ('LC activity') varied characteristically with states of wake, NREMS and REMS, consistent with recent studies (**Fig. 1c**)[18,19]. LC activity was elevated during wakefulness, but it declined in NREMS to a lower baseline on top of which a fluctuating pattern appeared. In 10 animals with a dynamic range of relative fluorescence changes between 16.3 – 95.3 % (mean 41.6 ± 9.3 %) in the first 2 h of the light phase (ZT0-ZT2) and a histologically confirmed fiber positioning (**Fig. 1b**), LC fluctuations were present throughout NREMS bouts but were absent during REMS (**Fig. 1c**). Mean LC activity levels in ZT0-ZT2 declined

129 progressively from wakefulness to NREMS and REMS (**Fig. 1d**) (for statistical details in all figures, see
130 **Supplementary Table 1**). However, activity levels in NREMS varied widely, with 56.5 ± 11.4 %
131 overlapping with wakefulness (calculated up to the mean - 2 standard deviations of wake levels; **Fig.**
132 **1d, Extended Data Fig. 1b**). In mouse NREMS, the collective neuronal activity levels of the
133 noradrenergic LC could thus go as high as in some periods of wakefulness.

134 Elevated LC activity promotes arousability from NREMS[16], but the brain states underlying this
135 arousal-promoting action have not been systematically examined. The LC projects cortically and
136 subcortically, including into autonomic output centers[1,7], suggesting that LC regulates arousability
137 through coordinating brain-bodily arousal levels. We first confirmed that LC activity fluctuations
138 generated robust variations of free NA levels in forebrain. Dual fiber photometric measures based on
139 jGCaMP8s fluorescence in LC and on $GRAB_{NE1h}$ fluorescence[33] in thalamus confirmed phase-locked
140 variations in both signals (cross-correlation coeff. > 0.5) (**Extended Data Fig. 1c, d**). Furthermore, high
141 LC activity levels coincided with power declines in a NREMS-specific frequency band, the spindle-
142 containing σ (10 – 15 Hz) power band, whereas σ power rose during low LC activity levels (**Extended**
143 **Data Fig. 1e1**)[17-20]. LC activity and σ power were anticorrelated with a time lag of 2.1 ± 0.5 s (n = 10)
144 and showed side peaks at 48.3 ± 2.2 s (**Extended Data Fig. 1e2**, range 38.5 – 58.1 s, measured in n =
145 6/10 animals in which these side peaks were clearly detectable). Therefore, in line with recent
146 findings[17], LC activity transients generated robust NA release that activated thalamus through
147 depolarization and suppressed sleep spindles.

148 We next isolated LC activity transients and studied the associated brain states together with
149 heart rate as a measure of autonomic activation (**Fig. 1e, Extended Data Fig. 2**). We noted that 30.0
150 % of LC activity transients (1,081 of 3,853 detected cases in n = 10 animals) were accompanied by a
151 MA (**Fig. 1f**), recognizable by an EEG desynchronization and a concomitant EMG activity lasting ≤12
152 s[21,32,34]. LC activity transients during MA lasted longer and were larger than when there was no MA,
153 suggesting greater overall noradrenergic output (**Fig. 1g**, n = 10). We hence analyzed non-MA-
154 associated LC activity transients separately from MA-associated ones (**Fig. 1h**, n = 10). These non-MA-
155 associated transients were accompanied by a decrease in σ (10 – 15 Hz) power and an increased
156 heart rate, reflecting a coordinated thalamic and cardiac activation during continuous NREMS. MA-
157 associated LC transients similarly altered sigma power and heart rate, yet with larger effect size (**Fig.**
158 **1i**). However, the two types of LC activity transients coupled oppositely to low-frequency power
159 changes. Specifically, power in the δ range (1.5 – 4 Hz) showed a small positive increase for non-MA-
160 associated LC activity transients ($p = 0.035$, paired t-test, effect size $D = -1.02$, n = 10; **Fig. 1h, i**),
161 which indicates a period of cortical deactivation or recurrent 'downstates'[35]. The MA-associated
162 transient showed instead a pronounced decrease in δ power, which reflects a cortical activation.

163 Opposite dynamics were also obtained for the γ frequency band (60 – 80 Hz), another correlate of
164 cortical activation[36]. In the case of MAs, there were γ power increases that coincided with EMG
165 activity, a MA-defining feature. The EEG spectral dynamics across δ, σ and γ bands could be similarly
166 reproduced for the LFP recordings in the S1 area, which indicates that LC-associated brain state
167 dynamics involved local thalamocortical circuits (**Extended Data Fig. 3a, b**). Point-by-point analyses
168 strongly suggested that all EEG and LFP spectral power changes and the heart rate accelerations
169 were likely induced by LC activity starting less than 50 s from the peak rather than by divergent EEG
170 or LFP dynamics starting before (> 50 s before the peak) (**Fig. 1h, Extended Data Fig. 3a**). These
171 analyses demonstrate that LC activity transients during NREMS coordinate a previously undescribed
172 brain-bodily state, characterized by a combined cardiac and thalamic activation that is dissociated
173 from cortical activation. During this state, arousability was enhanced because MAs appeared
174 preferentially[18,21], which caused cortical activation.

175 **Low LC activity levels are required for transitions to REMS**

176 Low LC activity levels have been previously associated with NREMS-to-REMS transitions ('REMS
177 entries'), but the causal role of the natural activity troughs for REMS entries has not been tested
178 directly. As reported[18,19], we noted that these troughs were associated with REMS entries (n = 9) (**Fig.
179 2a**). We next optogenetically modified activity troughs specifically and bidirectionally in DBH-Cre
180 animals expressing the excitatory opsin channelrhodopsin-2 (ChR2) or the inhibitory opsin Jaws in LC
181 neurons[17]. We tested whether REMS entries no longer occurred when LC was activated at moments
182 of the troughs. Conversely, we inhibited LC when it normally reached high levels. We tracked LC
183 fluctuations on-line through monitoring the σ power dynamics in the S1 LFP. We had previously
184 demonstrated that such monitoring allows to reliably distinguish between high and low LC activity
185 levels[17].

186 We optogenetically activated LC in ChR2-expressing animals at moments of rising σ power
187 (corresponding to low LC activity levels, see also **Extended Data Fig. 1e1**) in the first 20 min of every
188 h during ZT1-ZT9, with corresponding sham stimulations (LEDs turned-off) in separate sessions (**Fig.
189 2b**)[17]. This reduced the time spent in REMS and the frequency of REMS entries compared to sham
190 periods, but did not alter the density of MAs (0.58 ± 0.08 / min vs 0.62 ± 0.14 /min, Wilcoxon's signed
191 rank test; p = 0.3; n = 9). Conversely, we expressed the orange light-activated chloride pump 'Jaws' in
192 DBH-Cre animals and inhibited LC at moments when it was naturally high. We verified the efficacy of
193 this inhibition in 2 DBH-Cre animals expressing Jaws in the LC and $GRAB_{NE1h}$ in the thalamus. Jaws-
194 inhibition of LC (with continuous light exposure[17]) decreased NA levels in baseline and reduced the
195 extent of NA decline during REMS (**Fig. 2c**). When we next inhibited LC as soon as we detected a
196 decline in σ power, we specifically increased REMS time and the frequency of REMS entries (**Fig. 2d**).

197 Therefore, an optogenetically imposed decrease in natural LC activity, such as it occurs in troughs,
198 was permissive for REMS entries, while an increase in LC activity suppressed such entries.
199 The propensity to enter REMS increases linearly with the time spent in NREMS, which reflects
200 its homeostatic regulation[37]. Furthermore, several REMS-regulating brain areas innervate the LC[38-41].
201 Therefore, it was important to test whether LC activity fluctuations show a homeostatic
202 downregulation in the course of NREMS that would eventually permit REMS entries. Contrary to this
203 possibility, mean LC activity levels across NREMS bouts remained stable until just before REMS onset,
204 arguing against homeostatic regulation (**Fig. 2e**). These experiments establish that LC activity
205 troughs, whether naturally occurring or optogenetically promoted, generated windows of
206 opportunity for REMS entries throughout the major time spent in NREMS.

207 **REMS restriction shows that LC activity fluctuations ruled the timing of REMS entries**

208 The alternation between high and low LC activity levels takes place on infraslow time intervals.
209 Therefore, the time it takes for LC activity to decay from high to low levels could determine the
210 duration of NREMS before a REMS entry becomes possible. Clarifying this possibility would indicate
211 that there is an ultradian time interval that models of the NREMS-REMS cycle would need to
212 integrate[42]. To test this, we sought to increase the frequency of REMS entries while monitoring their
213 timing relative to on-going LC activity. We developed a REMS restriction (REMS-R) method in mice
214 designed to maximally reduce time spent in REMS while preserving NREMS time. We used vibrating
215 motors taped to the animals' headstage to interrupt REMS in closed-loop feedback (**Fig. 3a**)[21].
216 Starting at ZT0, these motors vibrated after 2 s of automatically detected REMS. When interrupting
217 every detected entry into REMS over a 6-h period from ZT0-ZT6, we observed a strong increase in
218 attempts to enter REMS (**Fig. 3b**). No such increase was observed in baseline recordings or in yoked
219 control animals that were exposed to vibration signals derived from the animal in the neighboring
220 cage. The REMS-R further preserved homeostatic regulation of NREMS and induced a rebound REMS
221 (**Extended Data Fig. 4**).

222 We examined the timing of REMS entries with respect to fiber photometric measures of LC
223 activity during REMS-R in a separate group of 8 animals. The mean duration of REMS bouts during
224 the REMS-R was 8.9 ± 2.4 s (n = 8), similar to the recently reported values of another automated
225 REMS-R method[43]. During REMS-R, every REMS entry remained invariably preceded by a decline of
226 LC activity (**Fig. 3c**). Furthermore, although REMS-R shortened the time between consecutive REMS
227 entries, these remained locked to moments of low LC activity levels (**Fig. 3d**). Starting from the 4th h
228 of the REMS-R, the mean interval remained comparatively stable and settled at 48.2 ± 6.3 s at ZT6
229 (**Fig. 3e1**). To examine the importance of low LC activity levels for REMS entries, we calculated

230 corresponding values for the last 5 s before every REMS entry across the full time of REMS-R. We
231 found these levels to remain stably low and constant during the entire 6 h of REMS-R (**Fig. 3e2**). This
232 strongly suggests that the decline of LC activity to a minimal level remained obligatory for a REMS
233 entry to become possible, in spite of a substantial increase in the pressure to enter REMS. To directly
234 test whether LC activity could suppress REMS entries even when the pressure for REMS was
235 elevated, we combined optogenetic LC stimulation in ChR2-expressing DBH-Cre animals with REMS-R
236 (n = 6, **Fig. 3f**). LC was stimulated at 1 Hz for 20 min/h, known to suppress baseline REMS (see **Fig.**
237 **2b**). This LC stimulation also suppressed REMS entries during the entirety of the REMS-R, with sham
238 (LED-off) conditions showing no effect. This indicates that moderate levels of LC activity (1 Hz) can
239 override a high REMS pressure to suppress REMS entries.
240 The combined evidence of a novel REMS-R method together with LC activity monitoring or
241 optogenetic testing supports an obligatory role of LC activity decline in ruling REMS entries, even
242 under conditions of high REMS pressure. The infraslow time course of LC's natural alternation
243 between high and low activity levels thus presents a previously unrecognized time interval that
244 gatekeeps sleep's organization in NREMS-REMS cycles.
245
246 **LC activity fluctuations gatekeep the natural NREMS-REMS cycle duration**

247 The mechanisms regulating natural cycle length remain poorly understood, although
248 homeostatic mechanisms have been implied[42]. Here, we asked whether the LC-associated infraslow
249 activity fluctuations were relevant for natural cycle length in undisturbed mouse sleep[44]. In mouse,
250 times spent in NREMS between REMS vary in length from < 1 min to > 30 min[44]. To probe whether LC
251 inhibition can modify cycle length, we therefore aimed to identify the set of cycles with relatively
252 little variability in duration. Following previous investigations on the interrelationship between
253 NREMS and REMS duration in mouse sleep[44,45], we analyzed how the time spent in NREMS depended
254 on prior REMS time in the light phase (n = 17). This showed that long REMS bouts (> 120 s) were most
255 consistently followed by long NREMS bouts, whereas shorter (< 100 s) REMS bouts were followed by
256 variable times spent in NREMS (**Fig. 4a, b**). In undisturbedly sleeping Jaws-expressing DBH-Cre mice
257 (n = 7), we hence measured the duration of each REMS bout in real-time, and, once it lasted ≥ 120 s,
258 we triggered optogenetic inhibition of LC in a double closed-loop experimental design. The onset of
259 this inhibition was set 'early' (within 50-100 s after NREMS onset) or 'late' (after NREMS time lasting
260 twice the duration of the preceding REMS bouts ± 10 s) time points in NREMS, which allowed to
261 probe LC's role at different moments in the NREMS-REMS cycle. Sham (LED-off) sessions took place
262 interleaved with test (LED-on) sessions (see Methods). When LC inhibition started early in NREMS,
263 we observed no significant change in the frequency of REMS entries or in times spent in REMS (**Fig.**

264 **4c**). In contrast, when LC inhibition started late, repeated REMS entries took place almost twice as
265 frequently compared to Sham stimulation (**Fig. 4d**). We confirmed the efficiency of inhibition by
266 histological examination of the correct optic fiber location (**Extended Data Fig. 5a**). To obtain an
267 additional independent measure for this efficiency, we examined how the observed increases in
268 REMS transitions correlated with changes in sleep spindle densities (**Extended Data Fig. 5b**)[17]. This
269 yielded a positive correlation, which supported the idea that a more efficient optogenetic LC
270 inhibition allowed for a stronger augmentation of REMS entries. As a final control, we demonstrated
271 that mCherry-only-expressing controls (n = 7) did not change the frequency of REMS entries upon
272 light exposure (**Extended Data Fig. 5c**). Natural LC activity fluctuations are thus critical for the normal
273 NREMS-REMS-cycle, in part because they appeared to prevent precocious REMS entries late in the
274 cycle and prolonged the time spent in NREMS. In contrast, LC activity appears to play a minor role at
275 relatively early stages of the cycle, when a long REMS bout was just completed and for which a
276 refractory period has been proposed[44].

277 **A stimulus-enriched wake experience increased LC activity fluctuations in NREMS and disrupted its**
278 **architecture**

279 Given the implication of LC activity fluctuations for the NREMS-REMS cycle, modifications in
280 the strength of these fluctuations could powerfully disrupt sleep. A recent study found that acute
281 stress during wakefulness can severely perturb LC activity in subsequent NREMS[19], but stress effects
282 and alterations in sleep-wake behavior remain to be dissociated. Here, we subjected jGCaMP8s-
283 expressing DBH-Cre mice to two different 4 h-long sleep deprivation (SD) procedures from ZT0-ZT4.
284 One SD was achieved by the 'gentle handling' technique that prevented animals from falling sleep
285 while minimally disturbing their spontaneous activity patterns in the cage (**Fig. 5a**). The stimulus-
286 enriched SD (SSD) was instead paired with auditory and somatosensory stimuli, to which the animals
287 were not previously habituated and exposed to in an unpredictable manner, thus promoting LC
288 activation (**Fig. 5b**)[1]. Both SD and the SSD were carried out at least 10 d apart in groups of 4 animals.
289 Blood sampling immediately after the SSD in a separate group of animals revealed increases in
290 corticosterone levels compared to baseline (**Extended Data Fig. 6**), indicating elevation of stress
291 levels in addition to the sensory exposure, which strongly implicates LC[1,2]. The SD produced by gentle
292 handling instead does not increase corticosterone levels[46].

293 As evident from the two representative recordings of sleep-wake behavior immediately after
294 SD or SSD of the same animal (**Fig. 5a-c**), LC continued fluctuating between activity transients and
295 troughs during NREMS, yet with the former ones distinctly strengthened. Both SD and SSD resulted in
296 comparable increases in low-frequency power of the EEG δ (1.5 – 4 Hz) band, indicating that the
297 homeostatic pressure to sleep had become elevated similarly in response to the 4-h wake time (**Fig.**

298 **5d**). Remarkably, the density of MAs changed in opposite directions for SSD compared to SD. SD
299 decreased MA frequency in subsequent NREMS, consistent with homeostatic sleep consolidation[32].
300 The SSD instead resulted in a marked increase in MA density and hence fragmented NREMS (**Fig. 5e**).
301 Furthermore, LC activity, measured in peak frequency (see Methods), was higher in the first h of SSD
302 compared to SD (**Fig. 5f**). Finally, the latency to REMS onset was increased in SSD compared to SD
303 and the number of REMS entries decreased within ZT4-ZT5 (**Fig. 5g**). In comparison to an extended
304 period of wakefulness, a stimulus-enriched wake experience combined with stress transiently
305 increased LC activity, disrupted sleep architecture for a post-SD/-SSD period of 1-2 h, and
306 antagonized the homeostatic effects of sleep consolidation.
307

308 **Inhibiting LC activity antagonized sleep disruptions induced by a stimulus-enriched wake**
309 **experience**

310 We examined the role of LC activity fluctuations in the SSD-induced sleep disruptions. First, we
311 determined the spectral profiles associated with high and low LC activity levels, as done for baseline
312 recordings (see **Fig. 1h, i**). LC activity transients remained associated with characteristic spectral
313 changes in the EEG for MA-associated events, however, increases in δ (1.5 – 4 Hz) power for non-MA
314 associated events were suppressed (**Fig. 6a**) in comparison to the SD condition (n = 7, paired t-test, p
315 = 0.038, effect size D = -1.42). All REMS entries also remained invariably associated with LC activity
316 declines (n = 7, **Fig. 6b**). Second, to causally test the consequences of elevated LC activity, we
317 subjected 9 Jaws-expressing DBH-Cre animals to two SSDs spaced at least 10 d apart, of which one
318 was followed by 1 or 2 h of Jaws-mediated bilateral inhibition of LC, the other one by LED-off (sham)
319 exposure, in a counterbalanced manner. LC inhibition attenuated the fragmentation of NREMS and
320 shortened REMS onset latency (**Fig. 6c**). LC's activity fluctuations in NREMS thus depend on the type
321 of wake experience and their modification can increase spontaneous arousability and delay REMS.
322 These data suggest that abnormal LC activity fluctuations can be causally involved in two important
323 hallmarks of deteriorated sleep quality.

324 **Discussion**

325 We identify the noradrenergic LC as a gatekeeper for the organization of mammalian sleep
326 into NREMS-REMS cycles. The underlying principle of action is LC's partitioning of NREMS into two
327 distinct brain and autonomic states, of which one was arousal-promoting, the other one permissive
328 for REMS (**Figure 7**). To date, we know much about the neural circuits underlying NREMS and REMS
329 individually, and both play important roles for sleep's restorative and memory-promoting functions[47-
330 49]. In comparison, the circuit mechanisms that rule the alternation between NREMS and REMS have
331 remained open, despite pioneering modeling and experimental work[11,24,25,41,42,50]. The identification

332 of the LC as a gatekeeper for the NREMS-REMS cycle is conceptually novel because it points to an
333 upstream oscillator-like mechanism that sets the time windows for the operation of NREM- or REMS-
334 regulating circuits. We also demonstrate that disrupting this gatekeeper fragmented sleep and
335 disrupted the NREMS-REMS cycle, and that it could override the consolidating effects of NREMS
336 homeostasis.

337 The LC was included as a REMS-off (that is, REMS-suppressing) brain area in the first
338 theoretical models for the NREMS-REMS cycle[24,25], which has been supported experimentally[17-19].
339 Through timing optogenetic interference to LC's natural activity fluctuations, we show here that LC
340 plays a dual role, suppressing REMS on the one hand, and setting the moments when REMS entries
341 are permitted on the other hand[25,42]. LC's permissive role adds an infraslow periodicity to the
342 architectural control of the NREMS-REMS cycle, defining recurring moments during which a REMS
343 entry is possible[42]. A possible advantage of LC's permissive role is an adaptability of NREM-REMS
344 cycle duration to circadian and homeostatic regulation, developmental state, metabolic and
345 emotional conditions, all of which shape the mammalian NREMS-REMS cycle across the lifespan[51].
346 Our study opens the way to explore these possibilities, for example by investigating how infraslow LC
347 activity fluctuations interplay with REMS-promoting areas in hypothalamic, brainstem, or mesolimbic
348 circuits.

349 This study further shows that unique brain and autonomic states associated with LC activity
350 fluctuations are core for the functional partitioning of NREMS. Following earlier work[16-18,22], we find
351 that LC activity transients acted in an arousal-promoting manner for the autonomic nervous system
352 (through accelerating heart rate) and for thalamic sleep spindle-generating circuits (through
353 suppressing sleep spindles)[17]. This is in line with an LC promoting arousal during NREMS.
354 Unexpectedly, we identify a cortical 'sleep-like' EEG or LFP activity that coincided with thalamic and
355 cardiac activation, suggesting that LC-linked arousal promotion involved subcortical but not cortical
356 areas. We show this subcortical arousal here for the sensory thalamus, but we speculate that other
357 areas strongly innervated by LC, such as midbrain and cerebellum[52], as well as other REMS-regulating
358 areas[7], might also be recruited, which could underlie the prevention of entries into REMS. In support
359 of a subcortically delimited action of LC, a functional imaging study in anesthetized rats indicated
360 that low-frequency optogenetic LC stimulation increased BOLD signals in the thalamus but not in the
361 cortex[53]. Furthermore, a consistent thalamic activation yet a variable cortical involvement was
362 identified via intracranial recordings for MAs in human NREMS[54]. Our analysis thus advances a circuit
363 foundation for a heterogeneity of aroused brain states in which wake- and sleep-related brain
364 activity can coexist. This will be relevant in dissecting the temporal sequence of arousal processes to
365 full wakefulness[55] and its possible dysfunction in disorders of arousals[56].

366 We further propose that the spectral and autonomic profile of LC activity is valuable in
367 identifying the diversity of arousals in the human sleep EEG. There are established arousal scoring
368 guidelines for human sleep[57], nevertheless, there remain EEG signatures for which the relationship to
369 arousal remains debated[23]. One example is a singular, large low-frequency EEG wave that is
370 prominent in human NREMS stage 2, referred to as 'K-complex'[58]. K-complexes are associated with
371 small but consistent increases in heart rate[59,60], yet they have been variably described as sleep-
372 protecting or arousal-related EEG hallmarks[58]. The data we present now indicate that increases in
373 low-frequency activity in the EEG can be a forebrain manifestation of activated brainstem arousal
374 circuits, which is in line with suggestions on the origins of K-complexes based on EEG source
375 analyses[61]. We suggest that some K-complexes in human sleep should be examined with respect to a
376 possible implication of LC activity in human NREMS. A recent study using pupillometry as a proxy for
377 LC activity in human sleep demonstrates that such progress is in reach[60].
378 Possible neural mechanisms by which LC activity activates the thalamus while promoting low-
379 frequency activity in the cortex can be derived from available knowledge on NA's actions within
380 thalamocortical circuits. Single LC unit recordings from rats in NREMS showed that individual spikes
381 are phase-locked to cortical slow (low-frequency) waves[13], while only high-frequency LC stimulation
382 activates the cortex[53]. Therefore, the NA release generated by minor neuronal discharge typical for
383 NREMS appears insufficient to disrupt the bistability of cortical up and down states, while it
384 depolarizes thalamocortical and thalamic reticular neurons and suppresses burst firing[17]. An
385 excitatory drive to the cortex that would result from enhanced thalamic output could prompt
386 switches between up and down states of cortical circuits[62], which would manifest as a transient
387 increase in low-frequency power. Once LC activity transients are longer or larger, as is for example
388 the case after SSD, its impact on cortex could be elevated and low-frequency power become
389 suppressed. Other mechanisms involving target-specific synaptic release of NA and peptide
390 messengers need to be further tested[1].
391 The important role of LC activity fluctuations for the NREMS-REMS cycle could be
392 demonstrated by asking how frequently entries from NREMS to REMS could be maximally permitted.
393 For this, we developed a specific REMS-R procedure as a next-level refinement of automated
394 approaches for REMS restriction[43]. This allowed to directly visualize that LC activity fluctuations
395 persisted even during high REMS pressure and that every REMS entry coincided with an invariable,
396 low, LC activity. Minimal, non-reducible time intervals were previously reported in REMS-restriction
397 protocols of similar duration[63,64], yet we provide here a first mechanistic basis that raises novel
398 questions about the role of this minimal duration. We cannot currently exclude that mechanisms
399 besides LC play a role, but we note that the noradrenergic LC is implied in neuronal, glial, and
400 vascular signaling mechanisms in the brain[7], all of which might take time to complete in NREMS

401 before REMS can start. We further note that REMS entries occurred in an almost oscillatory-like
402 manner in the last hours of the REMS-R, during which REMS pressure became excessively high. In
403 reptile sleep, alternations between NREM- and REMS-like states recur periodically on the infraslow
404 time scale[51,65]. We think that the infraslow time scale could be an evolutionarily conserved time
405 interval for the NREMS-REMS cycle over which a gatekeeping mechanism evolved later to adapt the
406 NREMS-REMS cycle to a variety of physiological needs.

407 An aversive or stressful experience in humans may disrupt sleep, for example by fragmenting
408 sleep and by suppressing REMS[66,67]. Several recent studies have identified the LC to be involved in
409 sleep disruptions preceded by acute stressful experiences[19,68], illustrating the growing recognition of
410 neural circuits involving monoamine release as a source for sleep disturbances. As LC controls both,
411 spontaneous arousability and REMS gatekeeping, alterations in its activity could have significant
412 consequences. Indeed, we found that a transient negative wake experience was sufficient to disrupt
413 the balance of LC activity fluctuations towards sustained high levels of activity. The resulting sleep
414 fragmentation and delay in REMS onset could be attenuated by antagonizing these elevated levels of
415 LC activity. This establishes the LC as an area that makes sleep vulnerable to recent, even transient,
416 and moderately adverse wake experiences.

417 The study offers a neural mechanism relevant for the alternation of mammalian sleep between
418 states of NREMS and REMS. Beyond this fundamental insight, our work has opened a translational
419 research line that will strengthen the connection between rodent and human sleep because it
420 proposes novel testable biomarkers for LC activity in human sleep. Furthermore, elucidating the
421 origins of LC's gatekeeping role could shine light on certain NREMS functions that inevitably require
422 time or coordinated to complete before a transition to REMS can be made. The susceptibility of
423 sleep-active LC to the preceding wake experience further brings novel opportunities to elucidate
424 sleep disruptions that could be impacted by the diversity of our daily experiences.

425 **References**

426 1 Poe, G. R. *et al.* Locus coeruleus: a new look at the blue spot. *Nat Rev Neurosci* **21**, 644-659,
427 doi:10.1038/s41583-020-0360-9 (2020).

428 2 Aston-Jones, G. & Cohen, J. D. An integrative theory of locus coeruleus-norepinephrine
429 function: adaptive gain and optimal performance. *Annu Rev Neurosci* **28**, 403-450,
430 doi:10.1146/annurev.neuro.28.061604.135709 (2005).

431 3 Berridge, C. W. Noradrenergic modulation of arousal. *Brain Res Rev* **58**, 1-17,
432 doi:10.1016/j.brainresrev.2007.10.013 (2008).

433 4 Rajkowski, J., Kubiak, P. & Aston-Jones, G. Locus coeruleus activity in monkey: phasic and
434 tonic changes are associated with altered vigilance. *Brain Res Bull* **35**, 607-616,
435 doi:10.1016/0361-9230(94)90175-9 (1994).
436 5 Reimer, J. *et al.* Pupil fluctuations track rapid changes in adrenergic and cholinergic activity in
437 cortex. *Nat Commun* **7**, 13289, doi:10.1038/ncomms13289 (2016).
438 6 Saper, C. B., Fuller, P. M., Pedersen, N. P., Lu, J. & Scammell, T. E. Sleep state switching.
439 *Neuron* **68**, 1023-1042, doi:10.1016/j.neuron.2010.11.032 (2010).
440 7 Osorio-Forero, A., Cherrad, N., Banterle, L., Fernandez, L. M. J. & Lüthi, A. When the locus
441 coeruleus speaks up in sleep: recent insights, emerging perspectives. *Int J Mol Sci* **23**,
442 doi:10.3390/ijms23095028 (2022).
443 8 Morris, L. S., McCall, J. G., Charney, D. S. & Murrough, J. W. The role of the locus coeruleus in
444 the generation of pathological anxiety. *Brain Neurosci Adv* **4**, 2398212820930321,
445 doi:10.1177/2398212820930321 (2020).
446 9 Yu, X., Franks, N. P. & Wisden, W. Sleep and sedative states induced by targeting the
447 histamine and noradrenergic Systems. *Front Neural Circuits* **12**, 4,
448 doi:10.3389/fncir.2018.00004 (2018).
449 10 Chu, N. S. & Bloom, F. E. Activity patterns of catecholamine-containing pontine neurons in
450 the dorso-lateral tegmentum of unrestrained cats. *J Neurobiol* **5**, 527-544,
451 doi:10.1002/neu.480050605 (1974).
452 11 Hobson, J. A., McCarley, R. W. & Wyzinski, P. W. Sleep cycle oscillation: reciprocal discharge
453 by two brainstem neuronal groups. *Science* **189**, 55-58, doi:10.1126/science.1094539 (1975).
454 12 Aston-Jones, G. & Bloom, F. E. Activity of norepinephrine-containing locus coeruleus neurons
455 in behaving rats anticipates fluctuations in the sleep-waking cycle. *J Neurosci* **1**, 876-886,
456 doi:10.1523/JNEUROSCI.01-08-00876.1981 (1981).
457 13 Eschenko, O., Magri, C., Panzeri, S. & Sara, S. J. Noradrenergic neurons of the locus coeruleus
458 are phase locked to cortical up-down states during sleep. *Cereb Cortex* **22**, 426-435,
459 doi:10.1093/cercor/bhr121 (2012).
460 14 Swift, K. M. *et al.* Abnormal locus coeruleus sleep activity alters sleep signatures of memory
461 consolidation and impairs place cell stability and spatial memory. *Curr Biol* **28**, 3599-3609
462 e3594, doi:10.1016/j.cub.2018.09.054 (2018).
463 15 Carter, M. E. *et al.* Tuning arousal with optogenetic modulation of locus coeruleus neurons.
464 *Nat Neurosci* **13**, 1526-1533, doi:10.1038/nn.2682 (2010).
465 16 Hayat, H. *et al.* Locus coeruleus norepinephrine activity mediates sensory-evoked
466 awakenings from sleep. *Sci Adv* **6**, eaaz4232, doi:10.1126/sciadv.aaz4232 (2020).

467 17 Osorio-Forero, A. *et al.* Noradrenergic circuit control of non-REM sleep substates. *Curr Biol*
468 **31**, 5009-5023 e5007, doi:10.1016/j.cub.2021.09.041 (2021).
469 18 Kjaerby, C. *et al.* Memory-enhancing properties of sleep depend on the oscillatory amplitude
470 of norepinephrine. *Nat Neurosci* **25**, 1059-1070, doi:10.1038/s41593-022-01102-9 (2022).
471 19 Antila, H. *et al.* A noradrenergic-hypothalamic neural substrate for stress-induced sleep
472 disturbances. *Proc Natl Acad Sci U S A* **119**, e2123528119, doi:10.1073/pnas.2123528119
473 (2022).
474 20 Fernandez, L. M. J. & Lüthi, A. Sleep spindles: mechanisms and functions. *Physiol Rev* **100**,
475 805-868, doi:10.1152/physrev.00042.2018 (2020).
476 21 Cardis, R. *et al.* Local cortical arousals and heightened (somato)sensory arousability during
477 non-REM sleep of mice in chronic pain. *Elife* **10**, e65835, doi:10.7554/eLife.65835 (2021).
478 22 Lecci, S. *et al.* Coordinated infra-slow neural and cardiac oscillations mark fragility and offline
479 periods in mammalian sleep. *Sci. Adv.* **3**, e1602026, doi:10.1126/sciadv.1602026 (2017).
480 23 Halasz, P., Terzano, M., Parrino, L. & Bodizs, R. The nature of arousal in sleep. *J Sleep Res* **13**,
481 1-23, doi:10.1111/j.1365-2869.2004.00388.x (2004).
482 24 McCarley, R. W. & Hobson, J. A. Neuronal excitability modulation over the sleep cycle: a
483 structural and mathematical model. *Science* **189**, 58-60, doi:10.1126/science.1135627 (1975).
484 25 Brown, R. E., Basheer, R., McKenna, J. T., Strecker, R. E. & McCarley, R. W. Control of sleep
485 and wakefulness. *Physiol Rev* **92**, 1087-1187, doi:10.1152/physrev.00032.2011 (2012).
486 26 Spiegel, R. & DeVos, J. E. Central effects of guanfacine and clonidine during wakefulness and
487 sleep in healthy subjects. *Br J Clin Pharmacol* **10**, 165S-168S, doi:10.1111/j.1365-
488 2125.1980.tb04925.x (1980).
489 27 Nicholson, A. N. & Pascoe, P. A. Presynaptic alpha$_2$-adrenoceptor function and sleep in man:
490 studies with clonidine and idazoxan. *Neuropharm* **30**, 367-372, doi:10.1016/0028-
491 3908(91)90062-g (1991).
492 28 Koshmanova, E. *et al. In vivo* locus coeruleus activity while awake is associated with REM
493 sleep quality in healthy older individuals. *bioRxiv*, doi:10.1101/2023.02.10.527974 (2023).
494 29 Vanderheyden, W. M., Poe, G. R. & Liberzon, I. Trauma exposure and sleep: using a rodent
495 model to understand sleep function in PTSD. *Exp Brain Res* **232**, 1575-1584,
496 doi:10.1007/s00221-014-3890-4 (2014).
497 30 Van Someren, E. J. W. Brain mechanisms of insomnia: new perspectives on causes and
498 consequences. *Physiol Rev* **101**, 995-1046, doi:10.1152/physrev.00046.2019 (2021).
499 31 Zhang, Y. *et al.* Fast and sensitive GCaMP calcium indicators for imaging neural populations.
500 *Nature*, doi:10.1038/s41586-023-05828-9 (2023).

501 32 Franken, P., Malafosse, A. & Tafti, M. Genetic determinants of sleep regulation in inbred
502 mice. *Sleep* **22**, 155-169 (1999).
503 33 Feng, J. *et al.* A genetically encoded fluorescent sensor for rapid and specific *in vivo* detection
504 of norepinephrine. *Neuron* **102**, 745-761 e748, doi:10.1016/j.neuron.2019.02.037 (2019).
505 34 Lüthi, A., Franken, P., Fulda, S., Siclari, F., Van Someren E.J.W. Do all noradrenaline surges
506 disrupt sleep? *Nat Neurosci* **26**, 955-956, doi:10.1038/s41593-023-01313-8 (2023).
507 35 Vyazovskiy, V. V. & Harris, K. D. Sleep and the single neuron: the role of global slow
508 oscillations in individual cell rest. *Nat Rev Neurosci* **14**, 443-451, doi:10.1038/nrn3494 (2013).
509 36 Buzsáki, G. *Rhythms of the brain*. (Oxford University Press, 2006).
510 37 Franken, P. Long-term vs. short-term processes regulating REM sleep. *J Sleep Res* **11**, 17-28
511 (2002).
512 38 Luppi, P. H. *et al.* Paradoxical (REM) sleep genesis: the switch from an aminergic-cholinergic
513 to a GABAergic-glutamatergic hypothesis. *J Physiol Paris* **100**, 271-283,
514 doi:10.1016/j.jphysparis.2007.05.006 (2006).
515 39 Weber, F. *et al.* Regulation of REM and non-REM sleep by periaqueductal GABAergic
516 neurons. *Nat Commun* **9**, 354, doi:10.1038/s41467-017-02765-w (2018).
517 40 Goutagny, R. *et al.* Role of the dorsal paragigantocellular reticular nucleus in paradoxical
518 (rapid eye movement) sleep generation: a combined electrophysiological and anatomical
519 study in the rat. *Neuroscience* **152**, 849-857, doi:10.1016/j.neuroscience.2007.12.014 (2008).
520 41 Stucynski, J. A., Schott, A. L., Baik, J., Chung, S. & Weber, F. Regulation of REM sleep by
521 inhibitory neurons in the dorsomedial medulla. *Curr Biol* **32**, 37-50 e36,
522 doi:10.1016/j.cub.2021.10.030 (2022).
523 42 Park, S. H. & Weber, F. Neural and homeostatic regulation of REM sleep. *Front Psychol* **11**,
524 1662, doi:10.3389/fpsyg.2020.01662 (2020).
525 43 Arthaud, S., Libourel, P. A., Luppi, P. H. & Peyron, C. Insights into paradoxical (REM) sleep
526 homeostatic regulation in mice using an innovative automated sleep deprivation method.
527 *Sleep* **43**, doi:10.1093/sleep/zsaa003 (2020).
528 44 Park, S. H. *et al.* A probabilistic model for the ultradian timing of REM sleep in mice. *PLoS*
529 *Comput Biol* **17**, e1009316, doi:10.1371/journal.pcbi.1009316 (2021).
530 45 Benington, J. H. & Heller, H. C. REM-sleep timing is controlled homeostatically by
531 accumulation of REM-sleep propensity in non-REM sleep. *Am J Physiol* **266**, R1992-2000,
532 doi:10.1152/ajpregu.1994.266.6.R1992 (1994).
533 46 Kopp, C., Longordo, F., Nicholson, J. R. & Lüthi, A. Insufficient sleep reversibly alters
534 bidirectional synaptic plasticity and NMDA receptor function. *J Neurosci* **26**, 12456-12465,
535 doi:10.1523/JNEUROSCI.2702-06.2006 (2006).

536 47 Brodt, S., Inostroza, M., Niethard, N. & Born, J. Sleep-A brain-state serving systems memory
537 consolidation. *Neuron* **111**, 1050-1075, doi:10.1016/j.neuron.2023.03.005 (2023).
538 48 Morrison, M., Halson, S. L., Weakley, J. & Hawley, J. A. Sleep, circadian biology and skeletal
539 muscle interactions: Implications for metabolic health. *Sleep Med Rev* **66**, 101700,
540 doi:10.1016/j.smrv.2022.101700 (2022).
541 49 Oesch, L. T. & Adamantidis, A. R. How REM sleep shapes hypothalamic computations for
542 feeding behavior. *Trends Neurosci* **44**, 990-1003, doi:10.1016/j.tins.2021.09.003 (2021).
543 50 Hayashi, Y. *et al.* Cells of a common developmental origin regulate REM/non-REM sleep and
544 wakefulness in mice. *Science* **350**, 957-961, doi:10.1126/science.aad1023 (2015).
545 51 Yamazaki, R. *et al.* Evolutionary origin of distinct NREM and REM sleep. *Front Psychol* **11**,
546 567618, doi:10.3389/fpsyg.2020.567618 (2020).
547 52 Schwarz, L. A. *et al.* Viral-genetic tracing of the input-output organization of a central
548 noradrenaline circuit. *Nature* **524**, 88-92, doi:10.1038/nature14600 (2015).
549 53 Grimm, C. *et al.* Locus Coeruleus firing patterns selectively modulate brain activity and
550 dynamics. *BioRxiv*, doi:10.1101/2022.08.29.505672 (2022).
551 54 Peter-Derex, L., Magnin, M. & Bastuji, H. Heterogeneity of arousals in human sleep: A stereo-
552 electroencephalographic study. *Neuroimage* **123**, 229-244,
553 doi:10.1016/j.neuroimage.2015.07.057 (2015).
554 55 Setzer, B. *et al.* A temporal sequence of thalamic activity unfolds at transitions in behavioral
555 arousal state. *Nat Commun* **13**, 5442, doi:10.1038/s41467-022-33010-8 (2022).
556 56 Castelnovo, A., Lopez, R., Proserpio, P., Nobili, L. & Dauvilliers, Y. NREM sleep parasomnias as
557 disorders of sleep-state dissociation. *Nat Rev Neurol* **14**, 470-481, doi:10.1038/s41582-018-
558 0030-y (2018).
559 57 Berry, R. *et al. The AASM Manual for the scoring of sleep and associated events : rules,*
560 *terminology and technical specifications.*, Vol. Version 2.5 (American Academy of Sleep
561 Medicine, 2018).
562 58 Halász, P. The K-complex as a special reactive sleep slow wave - a theoretical update. *Sleep*
563 *Med Rev* **29**, 34-40 (2016).
564 59 Sforza, E., Jouny, C. & Ibanez, V. Cardiac activation during arousal in humans: further
565 evidence for hierarchy in the arousal response. *Clin Neurophysiol* **111**, 1611-1619,
566 doi:10.1016/s1388-2457(00)00363-1 (2000).
567 60 Carro-Dominguez, M., Huwiler, S., Oberlin, S., Oesch T.L., Badii, G., Lüthi, A., Wenderoth, N.,
568 Meissner, S.N., Lustenberger C. Pupil size reveals arousal level dynamics in human sleep.
569 *Biorxiv* (2023).

570 61 Siclari, F. *et al.* Two distinct synchronization processes in the transition to sleep: a high-
571 density electroencephalographic study. *Sleep* **37**, 1621-1637, doi:10.5665/sleep.4070 (2014).
572 62 Shu, Y., Hasenstaub, A. & McCormick, D. A. Turning on and off recurrent balanced cortical
573 activity. *Nature* **423**, 288-293, doi:10.1038/nature01616 (2003).
574 63 Benington, J. H., Woudenberg, M. C. & Heller, H. C. REM-sleep propensity accumulates
575 during 2-h REM-sleep deprivation in the rest period in rats. *Neurosci Lett* **180**, 76-80,
576 doi:10.1016/0304-3940(94)90917-2 (1994).
577 64 Endo, T., Schwierin, B., Borbély, A. A. & Tobler, I. Selective and total sleep deprivation: effect
578 on the sleep EEG in the rat. *Psychiatry Res* **66**, 97-110, doi:10.1016/s0165-1781(96)03029-6
579 (1997).
580 65 Shein-Idelson, M., Ondracek, J. M., Liaw, H. P., Reiter, S. & Laurent, G. Slow waves, sharp
581 waves, ripples, and REM in sleeping dragons. *Science* **352**, 590-595,
582 doi:10.1126/science.aaf3621 (2016).
583 66 Deliens, G., Gilson, M. & Peigneux, P. Sleep and the processing of emotions. *Exp Brain Res*
584 **232**, 1403-1414, doi:10.1007/s00221-014-3832-1 (2014).
585 67 Wassing, R. *et al.* Restless REM sleep impedes overnight amygdala adaptation. *Curr Biol* **29**,
586 2351-2358 e2354, doi:10.1016/j.cub.2019.06.034 (2019).
587 68 Lo, Y., Yi, P. L., Hsiao, Y. T. & Chang, F. C. Hypocretin in locus coeruleus and dorsal raphe
588 nucleus mediates inescapable footshock stimulation (IFS)-induced REM sleep alteration.
589 *Sleep* **45**, doi:10.1093/sleep/zsab301 (2022).
590 69 Fernandez, L. M. *et al.* Thalamic reticular control of local sleep in sensory cortex. *Elife* **7**,
591 e39111, doi:10.7554/eLife.39111 (2018).
592 70 Owen, S. F. & Kreitzer, A. C. An open-source control system for in vivo fluorescence
593 measurements from deep-brain structures. *J Neurosci Methods* **311**, 170-177,
594 doi:10.1016/j.jneumeth.2018.10.022 (2019).
595 71 Sherathiya, V. N., Schaid, M. D., Seiler, J. L., Lopez, G. C. & Lerner, T. N. GuPPy, a Python
596 toolbox for the analysis of fiber photometry data. *Sci Rep* **11**, 24212, doi:10.1038/s41598-
597 021-03626-9 (2021).
598 72 Yuzgec, O., Prsa, M., Zimmermann, R. & Huber, D. Pupil Size Coupling to Cortical States
599 Protects the Stability of Deep Sleep via Parasympathetic Modulation. *Curr Biol* **28**, 392-400
600 e393, doi:10.1016/j.cub.2017.12.049 (2018).
601
602
603
604

605 **Materials and Methods**

606 **ANIMALS AND HUSBANDRY**

607 The study used two mouse lines - the C57BL/6J line and the B6.FVB(Cg)-Tg(Dbh-
608 cre)KH212Gsat/Mmucd (MMRRC Stock#036778-UCD) line, referred to here as DBH-Cre line, that was
609 originally provided to us by David McCormick and Paul Steffan, University of Oregon. Mice were bred
610 on a C57BL/6J background and housed in a humidity- and temperature-controlled animal house with
611 a 12 h / 12 h light-dark cycle (lights on at 9 am, corresponding to ZT0). Food and water were available
612 *ad libitum* throughout all experiments. For viral injections, 3- to 10-week-old mice of either sex were
613 transferred to a housing cabinet in a P2 safety level room, where they stayed from 1 d before to 3 d
614 after the viral injection. They were then transferred to the sleep-wake recording room and left to
615 recover for ≥ 1 week before undergoing the implantation surgery, after which they were single-
616 housed in standard-sized cages. The grids on top of the cage were removed and replaced by 30 cm-
617 high Plexiglass walls. Fresh food was regularly placed on the litter and the water bottle inserted
618 through a hole in the cage wall. Objects (tissues, paper rolls, ping-pong balls) were given for
619 enrichment.

620 In total, 10 DBH-Cre mice were used for two 12-h baseline sleep recordings in the light phase in
621 combination with fiber photometry under undisturbed conditions. One animal was excluded because
622 the dynamic range of the fluorescent signal ($\Delta F/F_0$ < 15%, see below). Additionally, two of these 2
623 DBH-Cre animals were used for combined fiber photometric monitoring of LC activity and NE levels,
624 these were included in the analysis of LC fluorescence across wake, NREMS, REMS. For combined LC
625 optogenetic inhibition with fiber photometric monitoring of NE release, 2 DBH-Cre animals were
626 used. Of the 10 DBH-Cre animals included for fiber photometric monitoring of LC activity, 8 were
627 used for 1-2 sessions of REMS-R in combination with fiber photometric monitoring of LC activity, and
628 9 underwent 1-2 sessions of SD and one session of SSD in combination with fiber photometric
629 monitoring of LC activity. Animals in which the dynamic range of fluorescence fell < 15% during
630 repeated fiber photometric sessions were no longer included in the analysis of LC activity. 9 DBH-Cre
631 mice for optogenetic stimulation and 9 DBH-Cre mice for optogenetic inhibition during different
632 phases of the infraslow fluctuation in σ power were already used in an earlier study and re-analyzed
633 here[17]. Seven DBH-Cre mice were used for optogenetic inhibition early or late in the NREMS-REMS
634 cycle, and an additional 7 were used for control viral injections. For the analysis of the statistics of
635 the NREMS-REMS cycle, baseline or sham sleep recordings from these 14 animals in the light phase,
636 plus additionally 3 animals otherwise not included in these experiments, were included. For the
637 validation of the REMS-R procedure alone, 9 C57BL/6J animals were used. For REMS-R in
638 combination with optogenetic stimulation, 6 DBH-Cre animals were used. 9 animals were used for
639 SSD in combination with optogenetic LC inhibition. A separate group of 8 animals were used for

640 quantification of corticosterone levels at ZT4 in baseline and after SSD. All experiments were
641 conducted in accordance with the Swiss National Institutional Guidelines on Animal Experimentation
642 and were approved by the Swiss Cantonal Veterinary Office Committee for Animal Experimentation.
643
644 **VIRAL VECTORS AND INJECTIONS**
645 General and local anesthesia, analgesia, temperature control, stereotaxic fixation and drilling of
646 craniotomies for injections of viral vectors were as described[17]. For fiber photometric monitoring,
647 DBH-Cre mice were unilaterally injected over the right LC (L 1.05; AP -5.4; DV -3.2) with AAV5-hSyn1-
648 dlox-jGCaMP8s-dlox-WPRE-SV40p(A) (titer 5.8Ex10^{12} vg/ml, 300nL, unilateral, Viral Vector Facility
649 (VVF) Zürich) at an injection rate of 50-100 nL/min using a thin glass pipette (5-000-1001-X,
650 Drummond Scientific) pulled on a vertical puller (Narishige PP-830), initially filled with mineral oil,
651 and backfilled with the virus-containing solution just prior to injection. For transfection of the LC for
652 optogenetics, viral vectors injected were ssAAV5/2-hEF1α-dlox-hChR2(H134R)_mCherry(rev)-dlox-
653 WPRE-hGHp(A) (9.1x10^{12} vg/ml, 0.8 – 1 µL, unilateral, VVF Zürich) or ssAAV-5/2-hSyn1-dlox-
654 Jaws_KGC_EGFP_ERES(rev)-dlox-WPRE-bGHp(A)-SV40p(A) (6.4x10^{12} vg/ml, 300 nL bilateral, VVF
655 Zürich). The control virus for Jaws experiments was ssAAV-5/2-EF1α-dlox-mCherry(rev)-dlox-WPRE-
656 bGHp(A) (7.3x10^{12} vg/ml, 300 nL bilateral, VVF Zürich). For monitoring of free NA levels, ssAAV9/2-
657 hSyn1-GRAB_NE1h-WPRE-hGHp(A) (7.2x10^{12} vg/ml; VVF Zürich) was injected unilaterally in primary
658 somatosensory thalamus (500 nL; L 2.0; AP -1.6; D -3.0), as described before [17]. Two animals each
659 were dually injected for combined expression of jGCaMP8s and $GRAB_{NE1h}$ or Jaws and $GRAB_{NE1h}$ in the
660 right hemisphere. After the injections, the incision was sutured and disinfected, and the animal was
661 supervised and given paracetamol at 2 mg / ml for the next 4 days.
662
663 **SURGERIES**
664 **Surgeries for sleep recordings.** Surgeries for implantation of electrodes for sleep-wake monitoring
665 were done at least 1 week after the viral injection. Following anesthesia induction (5% Isoflurane,
666 animals were gas-anesthetized (Isoflurane 1.5 – 2.5%) in a mixture of O_2 and N_2O. After analgesia
667 (Carprofen 5mg/kg i.p.) and disinfection, animals were fixed in a Kopf stereotax and injected into the
668 scalp with a mix of lidocaine (6 mg/kg)/bupivacaine (2.5 mg/kg). To expose the skull, the skin was
669 incised, and the bone scratched with a fresh scalpel blade to improve adhesion of the head implant.
670 Then, we drilled small craniotomies (0.3 – 0.5 mm) over left frontal and parietal bones and
671 positioned two conventional gold-coated copper-wire electrodes in contact with the dura mater for
672 EEG recordings. In case of unilateral LC injections, EEG electrodes were implanted contralaterally. On
673 the ipsilateral (right) side, high-impedance tungsten LFP microelectrodes (10–12 MΩ, 75-µm shaft
674 diameter, FHC) were implanted in the primary somatosensory cortex (L +3.0; AP -0.7; D -0.85) and

675 the hippocampus (L +2.0; AP -2.46; D -1.2 to -1.3). Additionally, as a neutral reference, a silver wire
676 (Harvard Apparatus) was inserted into the occipital bone over the cerebellum and two gold pellets
677 were inserted into the neck muscles for EMG recordings. All electrodes were fixed using Loctite
678 Schnellkleber 401 glue and soldered to a multisite connector (Barrettes Connectors 1.27 mm, male
679 connectors, Conrad). Animals were single housed after surgeries.
680 **Surgeries for fiber photometry recordings.** For fiber photometry, fiber implantation occurred
681 together with the surgical implantations for sleep recordings. Shortly, an optic fiber stub coupled to a
682 cannula (Doric Lenses, MFC_400/430-0.66_3.5mm_ZF1.25(G)_FLT) was implanted over the right LC (L
683 +0.9; AP -5.4; D -2.7) at an insertion speed of 1 mm/min using a Kopf stereotaxic holder, for 1 animal
684 the fiber was implanted with an angle of 20 degrees leading to a different set of coordinates (L +1.84;
685 AP -5.4; D -2.9). For dual fiber photometry, this procedure was repeated over the primary
686 somatosensory thalamus (L +1.8; AP -1.7; D-2.5), over which the fiber stub was vertically inserted.
687 Fibers were glued to the skull and were part of the dental cement structure holding the entire
688 implant into place.
689 **Surgeries for optogenetics.** For optogenetic stimulation of noradrenergic LC neurons, 4 mm-long
690 optic fibers were purchased pre-pared (MFC_200/250-0.66_4mm_ZF1.25(G)_FLT) or fabricated from
691 a multimode fiber (225 μm outer diameter, Thorlabs, BFL37-2000/FT200EMT) using the custom-
692 made procedure described in ref[17]. For optogenetic inhibition, 5 mm-long optic fibers attached to an
693 optic canula were used (CFMLC12L05, Thorlabs). The implantation coordinates for stimulation were
694 (L +0.9; AP -5.4; D -2.5 unilaterally in the right LC), while for inhibition two fibers were implanted
695 bilaterally using a 20° angle from the vertical with coordinates (L +/-1.84; AP -5.4; D -2.5) from
696 bregma. The emitted light intensity at the fiber tip was evaluated prior to implantation for every
697 fiber.
698
699 **RECORDING PROCEDURES AND PROTOCOLS**
700 **Sleep recordings**. Sleep recordings always took place within the animals' home cage. Once recovered
701 from surgery for > 1 week, animals were habituated to cabling to an ultrathin Intan SPI cable and
702 adaptor board via a custom-made support system (Homemade adapters containing an Omnetics
703 A79022-001 connector linked to a female Barrettes Connector from Conrad). These served as
704 intermediate between the head implant of the animal and the headstage (RHD2132 amplifier board)
705 that was connected to the Intan USB interface Acquisition Board (RHD2000). All signals (EEG frontal
706 and parietal, left and right EMG, S1 and CA1 LFPs) were acquired in unipolar mode at 1 kHz.
707 All recordings were done in the 12-h light phase (ZT0-ZT12). For closed-loop optogenetic stimulation
708 and inhibition sessions timed to the infraslow σ power fluctuations in NREMS, 2 sessions were done
709 per condition (Rising or declining σ power, Sham LED-off or Light stimulation). In experiments using

710 optogenetic stimulation or inhibition according to the infraslow phase, sessions were spaced by one
711 day and data meaned between sessions. For optogenetic inhibition timed to the early or the late
712 phase of the NREM-REMS cycle, 10 to 20 sessions per animal were recorded over 3 weeks' time. For
713 the two REMS-R sessions per animal, at least 2 interleaved days were given. Per animal, there were
714 1-2 SDs that were kept at least 7 days apart. The SSD was spaced apart from the SD sessions by at
715 least 7 days, and 10 days were given for two SSDs combined with LC optogenetic inhibition or sham
716 (LED-off) exposure. For details of the light exposure, see 'Optogenetic protocols'.
717 **Fiber photometry recordings**. Fiber photometry recording sessions took place at least one week
718 after surgery and >1 day apart. Two signal generators modulated the blue (465 nm) and the violet
719 (405 nm) LED of the Doric Fluorescence MiniCube LEDs (ilFMC4-G2_IE(400-410)_E(460-490)_F(500-
720 550)_S) using sinusoidal signals at 319 and 211 Hz, respectively. The combined modulated light was
721 then transmitted through a 400-µm-thick fiberoptic patchcord (MFP_400/430/1100-0.57_1m_FMC-
722 ZF1.25_LAF, Doric Lenses) to the implanted optic canula on the head of the animal. A photodetector
723 integrated into the MiniCube turned the emitted light from the fluorescent sensors into a current
724 signal that was fed into an analog signal of the Intan RHD2132 amplifier board as described
725 previously[17]. The measured power at the tip of the optic fiber was, for both wavelengths, 20 – 30 µW
726 ensuring minimal bleaching throughout the 12 h of recordings.
727 **Optogenetics protocols.** For optogenetic interference at different phases of the infraslow σ power
728 fluctuations, protocols were applied as described[17]. The optogenetic manipulations took place every
729 first 20 min/h from ZT1-ZT9. Stimulation sessions (with LED on) took place in exchange with sham
730 session (LED off). Entries into NREMS were detected online through setting a threshold for the low-
731 frequency (1 – 4 Hz) over θ (6 – 10 Hz) ratio for the differential frontal-parietal EEG signal and the
732 decline in the absolute EMG amplitude. Occasional brief interruptions in LED stimulation during
733 NREMS are due to a trespassing of that ratio, either caused by muscle twitches or spectral
734 fluctuations. Once in NREMS, σ power fluctuations were monitored online and increasing or
735 decreasing slopes detected through a machine-learning procedure[17]. For LC stimulation, we used 1
736 Hz pulses of 10 ms applied to a PlexBright Plexon BlueLED unit emitting 465 nm blue light at 2.8-3.2
737 mW intensity. For LC inhibition, we used continuous stimulation of an orange LED module (620 nm,
738 1.55 – 1.7 mW at the tip).
739 For optogenetic interference at different time points in the NREMS-REMS cycle, we used a closed-
740 loop algorithm to identify REM and NREMS based on the low-frequency (1 – 4 Hz) over θ (6 – 10 Hz)
741 ratio for the differential frontal-parietal EEG signal and the EMG activity based on 4-s windows with a
742 3 s overlap (i.e. updated every s), as previously described[21]. Upon online identification of long REMS
743 bouts (>120 s), 20-min continuous optogenetic inhibition started randomly after 50 – 100 s of NREMS
744 (*early inhibition*), or after twice the time of the identified REM bout (at least 240 s or 2 times the

745 duration of the preceding REMS bout) with a random 10-s jitter (*late inhibition*). The time points
746 chosen to start the early or the late inhibition were based on a previous study analyzing the
747 probabilities for REMS entries after a long REMS bout[44]. Several sessions were recorded so that we
748 collected around 10 episodes of long REM bouts per condition per animal.
749 For optogenetic inhibition after SSD (see below for procedure), LC was continuously inhibited for 1 or
750 2 h after the end of the SSD using continuous illumination. The stimulation started once a 10-s long
751 NREMS was automatically detected, using a closed-loop algorithm based on the low-frequency (1 – 4
752 Hz) over θ (6 – 10 Hz) ratio for the differential frontal-parietal EEG signal and the EMG activity. This
753 resulted in a mean of 36.3 ± 5.1 min and 34.5 ± 4.5 min of sleep/h of light stimulation for sham and
754 test conditions, respectively (n = 9). One additional animal was *post hoc* excluded from analysis
755 because it slept only ~5 min during the 2-h post SSD light exposure, which provided insufficient data
756 for analysis. Per animal, one SSD followed by LC inhibition and one SSD followed by Sham inhibition
757 was carried out in a counterbalanced design.
758
759 **BEHAVIORAL MANIPULATIONS**
760 **REMS restriction (REMS-R).** We used small vibrating motors (DC 3–4.2 V Button Type Vibration
761 Motor, diameter 11 mm, thickness 3 mm) that we fixed using double-sided tape to the end of the
762 recording cables, close to the animals' heads. The motors were driven to vibrate through a closed-
763 loop system using a Raspberry Pi[21]. Once the θ (6 – 10 Hz) / δ (1 – 4 Hz) ratio of the CA1 LFP signal
764 passed a threshold 1.5 for > 2 s and EMG activity declined below a threshold of 0.35 that was based
765 on the min/max normalization of the median log10 EMG activity/s, the motors vibrated for 2 s and
766 woke up the animal, as monitored by polysomnography. A control session for protocol
767 standardization was included in which the motor of an animal was activated based on the closed-
768 loop of the neighbor animal (yoked controls). The animals included only for the validation for the
769 REMS-R procedure were separate from the ones in which LC activity was monitored or
770 optogenetically altered during the REMS-R in terms of analysis. The REMS-R was carried out from
771 ZT0-ZT6 for all experiments except when REMS-R was combined with LC optogenetic stimulation.
772 Then, REMS-R lasted from ZT1-ZT9 and 20 min optogenetic stimulation was applied during NREM
773 sleep, as described above (optogenetic protocols).
774 **Gentle sleep deprivation (SD).** Animals were kept awake from ZT0-ZT4 while in their home cage and
775 tethered to the recording apparatus. One person supervised two animals at the time and added
776 nesting materials (pieces of Kleenex tissue) or gently interfered with the animals' spontaneous
777 behavior once it started adopting a sleeping posture[46]. For this, we used an ~30 cm-long stick
778 scotched to a ball of Kleenex tissue to gentle displace the litter around the nest or to wipe the wall of
779 the cage. The animal was never touched throughout the entire procedure.

780 **Stimulus-enriched sleep deprivation (SSD).** The animals were placed in a novel cage and subjected to
781 several manipulations every 20-30 min to touching (1-2 min), gentle cage shaking (5 min) or auditory
782 stimulation (knocking at the cage, 5 min) from ZT0-ZT4. Two animals were supervised per person.
783 These manipulations were paired one each for touching and cage shaking and auditory stimulation
784 and cage shaking, and once done the three together. At the end, animals were transferred back to
785 their home cage and left undisturbed. In animals used for fiber photometric recording of LC
786 fluorescence, one SSD was carried out. In animals in which LC was inhibited after SSD, two SSDs per
787 animal were carried out (one for sham LED-off inhibition, one for light inhibition). Corticosterone
788 measures were carried out at ZT4 for baseline (undisturbed) and SSD conditions per animal by
789 drawing tail vein blood samples. Samples were kept on ice in heparin-coated tubes and centrifuged
790 at 4° for 4 min 9,400xg. Plasma was extracted and corticosterone levels measured with the Enzo Life
791 Sciences kit (Catalog No. ADI-901-097).
792
793 **HISTOLOGY**
794 At the end of all the recording sessions the animal was injected i.p. with a lethal dose of
795 pentobarbital. The position of each LFP electrode was subsequently marked using electro-
796 coagulations (50 µA, 8 – 10 s). Afterwards, ~40 mL paraformaldehyde (4%) were perfused
797 intracardially at a rate of ~3 mL min^{-1}. The brains were then extracted and post-fixed for at least 24 h
798 in 4% PFA at 4°C. Subsequently, the tissue was sliced in 50 µm-thick (for brainstem) or 100 µm-thick
799 (for thalamus or cortex) sections using either a vibratome (Microtome Leica VT1000 S; speed: 0.25 –
800 0.5 mm s^{-1} and knife sectioning frequency: 65 Hz) or a freezing microtome (Microm). After cutting,
801 the slices were either directly mounted (using Mowiol as a mounting medium) or stored in 0.1 M PB.
802 Finally, we confirmed the anatomical location of the LFP and the viral-mediated expression of the
803 fluorescent proteins with a Nikon SMZ25 Stereomicroscope equipped with a Nikon DS-Ri2 16 Mpx
804 color camera. For a higher magnification image an Axiovision Imager Z1 (Zeiss) microscope was used
805 (objectives used EC-Plan Neofluar 2.5x/0.075 ∞/0.17, 5x/0.16 ∞/0.17, 10x/0.3 ∞/- or 20x/0.5
806 ∞/0.17).
807 For assessing the colocalization of jGCaMP8s expression with tyrosine hydroxylase (TH)
808 expression in the LC neurons, coronal brain sections 50 µm-thick (~-5.3 mm from bregma), were first
809 washed in 0.3% Triton in PBS 3 times, incubated in blocking solution of PBS 0.3 % and 2 % normal
810 goat serum for 1 h and then overnight with the primary antibody (mouse anti-TH antibody, dilution
811 1:2000, Immunostar, 22941) at 4 °C while on a shaker. After a total incubation for at least 12 h, the
812 slices were washed 3 times with PBS containing 0.3 % Triton. Afterwards, the secondary antibody
813 was added (1:100 donkey anti-mouse antibody coupled to Alexa Fluor 594, Invitrogen, A21203, in
814 PBS containing 0.3 % Triton) and the slices were incubated for 1-1.5 h at room temperature on a

shaking platform. At the end of the procedure the slices were rinsed with PB 0.1 M and mounted (using again Mowiol as a mounting solution). The images (red and green emission channels) were acquired using a confocal microscope (Leica Stellaris 8) equipped with a 63x oil objective (HC PL APO 63x/1.40 oil CS2).

ANALYSIS PROCEDURES

Sleep analysis.

Sleep scoring. We scored sleep stages in 4-s epoch using the EEG/EMG signals according to standard procedures using a custom-made semiautomated Matlab routine available on our Github Repository (https://github.com/Romain2-5/IntanLuthiLab). For every epoch, EEG was inspected for its spectral composition and the EMG for its level of activity. Wakefulness was scored when high-frequency phasic EEG activity coincided with strong EMG activity; NREMS was scored when high-amplitude low-frequency components, such as slow oscillations (0.5 – 1.5 Hz) and δ activity (1.5 – 4 Hz), and recurrent sleep spindles (10 – 15 Hz) appeared in combination with low muscle tone; REMS was scored whenever a θ peak (6 – 10 Hz) appeared and muscle atonia developed. For determining the exact onset of REMS, a thresholding of θ/δ power was used for the CA1 LFP signal (see Spectral dynamics below). For epochs at transitions, the vigilance state that covered more than half of the epoch (> 2 s) was scored. Microarousals were scored when maximally 3 wake epochs (≤ 12 s) showing both EEG desynchronization (predominance of faster, low-amplitude, over slower high-amplitude activity) and EMG activity appeared sequentially and were both preceded and followed by NREMS. An epoch was also scored as MA when wake activity (in both EEG and EMG) lasted < 2 s. For analysis of intervals between successive REMS episodes during REMS-R, the motor vibration signal was used. The interval between two successive REMS episodes was quantified at the time spent in NREM sleep (in seconds) between two successive motor onsets (for this analysis microarousals were considered as part of NREM sleep).

Spectral dynamics. The dynamics of spectral bands were calculated from the S1 and CA1 LFPs using wavelet transforms with Gabor-Morlet Kernels with 4 cycles of standard deviation for the Gaussian envelope at 0.1 Hz resolution. For spectral analysis involving S1 LFP signals or EEG, frequency bands analyzed were δ (1.5 – 4 Hz), θ (6 – 10 Hz), σ (10 – 15 Hz), β (16 – 25 Hz), γ (60 – 80 Hz). The hippocampal LFP was used for calculation of the ratio of a θ (6 – 10 Hz) over δ (1 – 4 Hz) ratio (θ/δ) in the CA1 LFP electrode, in which the δ band was started at 1 Hz for convenience. For band-defined dynamic changes, the S1 or EEG signal were first down-sampled from 1 kHz to 200 Hz, the Wavelet transform calculated within the desired frequency bands and collapsing the frequency dimension. The derived signals were down-sampled at 10 Hz and low-pass-filtered at a cut-off frequency of 0.1

849 Hz. The detection of individual spindles was calculated as previously described[17,69]. For the CA1
850 signal, a similar procedure was applied to obtain the ratio for θ/δ and a threshold of 1.5 was chosen
851 to define REMS onset around the previously defined manual transition. The dynamics of the EMG
852 were calculated as absolute values from the 0.1 Hz-filtered trace.
853 **Heart rate quantification**. Heart rate was quantified as described before using the R-R peaks
854 recorded by the EMG, using the square of its derivative and the Matlab FindPeaks function[17,21].
855 **Fiber photometric analysis.**
856 **Extraction of $\Delta F/F_0$ signals and baseline correction.** Using the modulated recorded photometry
857 signal, we demodulated two separate channels. A functional signal (from the blue excitation LED),
858 carrying the calcium-dependent activity, and an isosbestic, calcium-independent one (from the violet
859 excitation LED). We utilized the workflow and the MATLAB codes available as open source[70].
860 Afterwards, the $\Delta F/F_0$ signal was computed using as F_0 the fitted isosbestic signal, following the
861 procedure explained in ref[71].
862 For all analysis, fiber photometric signals were included in the analysis only if the dynamic range,
863 calculated between the minimum and the maximum of the signal within the first 2 h of the recording,
864 was > 15%. In the next paragraphs describing specific analyses, this extracted signal is referred to as
865 the 'LC signal'.
866 **All-points histograms.** We constructed all-points histograms from z-scored fiber photometric
867 datasets obtained from all 10 animals for the first 2 h of the light phase. Overlap between NREMS
868 and Wake period was calculated based on the number of data points in NREMS that are larger than
869 the mean minus 2 standard deviations of the levels in wakefulness.
870 **Analysis of LC peaks and LC activity transients**. The definition of the LC peaks and activity transients
871 are illustrated in **Extended Data Fig. 2** and are briefly summarized here. First, the LC signal was low-
872 pass-filtered at 0.5 Hz (FIR filter of order 100) and rectified by the lower envelope (96-s sliding
873 window) of the 0.1 Hz low-pass-filtered signal. Second, we detected the peaks in the rectified signal
874 using the FindPeaks function of Matlab®. We discarded all peaks within the 60 percentile of
875 prominence and used "halfheight" for the "WidthReference" parameter. From the rest of the peaks,
876 we discarded the peaks under 25% of the maximum prominence and 20% of the signal amplitude. All
877 MAs were included in these analyses.
878 Second, the LC activity transients in NREMS were defined as the fiber photometric signal events that
879 show a rapid onset and that could contain multiple peaks. These were identified from the LC peaks
880 within consolidated NREM sleep (>96 s of NREM sleep and after 1.5 times the time constant (Tau) of
881 lower envelope decay after wake periods of >60 s). The maximum peak within a window of 20 s was
882 defined as the transient peak. To define the start and the end of the transients we used the z-score
883 of the 100 s window around each transient peak. The start of the transient was defined as the first

884 peak within the derivate of the signals within the 10 s period before the transient peak. The end of
885 the transient was the moment when the signal reached 15% of the maximal value of the 100 s
886 window. The start and the onset of each activity transient were used to determine the duration and
887 the area of the activity transients.
888 For the analysis of LC peaks after SD and SSD, mean peak frequency values were calculated for equal
889 times spent in NREMS (12 bins for baseline conditions, 8 for the SD and SSD conditions).
890 **Cross-correlations between LC activity, NA levels, σ power.** Cross-correlations were calculated
891 analogously to the previous one done for NA fluctuations and σ power[17] using z-scored σ power and
892 LC signals, or the NA and LC signals, at 0.1-s resolution, for all NREMS bouts > 96 s, including MAs,
893 from ZT0-ZT12. A mean cross-correlation per animal was calculated and presented for the time
894 interval between -200 s to 200 s. In the case of the cross-correlations between LC activity and σ
895 power, the position of side peaks could be extracted in 6 out of 8 cases (based on the dynamic range
896 of the LC signal, see **Extended Data Fig. 1e2**). For the cross-correlation between NA and LC signals
897 (**Extended Data Fig. 1d**), the two animals with dually recorded fiber photometry were used. Cross-
898 correlations were then averaged across animals. A positive time lag indicates that the LC signal
899 increases preceded σ power decreases or NA increases. We refer to 'LC activity transients' as the
900 high LC activity levels that anticorrelate with the σ power and that appear on infraslow time intervals
901 (30 – 50 s).
902 **Spectral analysis around LC activity peaks.** Local maxima of the LC signals were defined using a 20-s
903 sliding window on the LC $\Delta F/F_0$ signal, excluding the ones falling within the initial decay of the fiber
904 photometric signal at transitions from Wake to NREMS. We then derived the z-scored spectral
905 dynamics for different frequency bands using the wavelet approached previously described (See
906 *Sleep Analysis - Spectral dynamics*) around these maxima from – 150 s to + 50 s. In a second step,
907 these peaks were classified according to whether or not they were associated with a MA (defined by
908 EEG/EMG activity as described in *Sleep Analysis – Sleep Scoring*) within 5 s around the peak.
909 Additionally, we calculated the absolute EMG activity and the z-scored heart rate within these
910 windows and repeated this analysis for both for the S1 LFP and the EEG during NREMS bouts for all
911 times. Mean amplitudes for the LC signal and for heart rate were calculated as the difference from
912 the peak time to the minimum value before the peak (-10 s to 0 s). Mean amplitudes for spectral
913 power bands were calculated from times 0 s to 1 s.
914 **Spectral analysis at REMS onset.** The exact timing of REMS onset was defined using a thresholding
915 for θ/δ at 1.5 using the CA1 LFP electrode. Using the parietal EEG electrode provided similar time
916 points. The dynamics for preceding NREMS were then obtained for the S1 LFP σ band and for the
917 low-pass filtered absolute EMG signal. For LC signals with high dynamic range, an inflection point
918 could be observed prior to REMS onset after which there was a further decrease to a new minimum

(see e.g. Fig. 2c). This inflection point was associated with a further increase in σ power and the onset of EMG decline, consistent with markers for 'Intermediate sleep'.

Sleep architecture analysis during LC optogenetic stimulation and inhibition. For LC stimulation or inhibition according to the phase of the σ power fluctuation, times spent in Wake, NREMS and REMS were calculated for the test or sham stimulation 20-min sessions and expressed in % of total time. Transitions were calculated as the number of REMS-epochs followed by NREMS. For LC inhibition at different moments in the NREMS-REMS cycle, a similar procedure was applied.

Mean LC activity in NREMS bouts. The LC fluorescent signal was extracted between REMS bouts lasting ≥ 12 s, z-scored for all NREMS including MAs, and plotted over normalized NREM time between the consecutive REM bouts. The derived signals were averaged based on the length of the preceding REM bout as previously done for similar purposes[44].

Quantification of rebound REMS after REMS-R. To demonstrate the efficiency of the REMS-R, we also quantified rebound REMS by calculating cumulative times spent in REMS during REMS-R and the 6 h – post REMS-R period.

LC signal analysis during REMS-R. To determine the relative level of LC activity prior to REMS entry during the REMS-R, we extracted bouts where a transition to REMS was present and preceded by at least 12 s of NREM sleep. The $\Delta F/F_0$ LC activity was then z-scored for each bout and we reported the mean $\Delta F/F_0$ value during the last 5 s before the transition to REMS.

LC stimulation during REMS-R. For each 20 min stimulation block (first 20 min of every h from ZT1–ZT9) during the REMS-R, we normalized the time in equal amounts of NREMS for the periods before, during and after stimulation (10 bins per block) and calculated the number of REM entries per min of NREMS. A similar approach was done to the analogous periods during sham stimulation, *ceteris paribus*, with the LEDs turned off.

STATISTICS

The statistics were done using Python, Matlab R2021a or R statistical language version 4.0.1. The normality of data distributions was assessed using the Shapiro–Wilk and Levene tests. In cases of normality violations, non-parametric Kruskal-Wallis and Wilcoxon tests were used. Datasets were collected in experimental designs allowing preferentially repeated measures and/or paired statistical analysis. Post-hoc analyses were done only when the one-way factor or the interaction between factors was significant ($p<0.05$). Bonferroni's correction for multiple comparisons was applied routinely, and the corrected α thresholds are given in the figure legends. Differences in the dynamics of power bands and heart rate were calculated using t-tests and correcting for multiple comparisons using False Discovery Rates (FDR) where the significant values satisfy $P(k) < 0.05 * k/2000$, where P is the vector of the ranked p values of the point-to-poitn t-test within the window (-150 s to 50 s at 10

954 Hz). In all figure legends, the statistical tests used are mentioned, while sample numbers and p values
955 are indicated directly in the figure panels. Details of all statistical tests and effect sizes are
956 summarized in **Supplementary Table 1**.
957
958
959
960
961
962

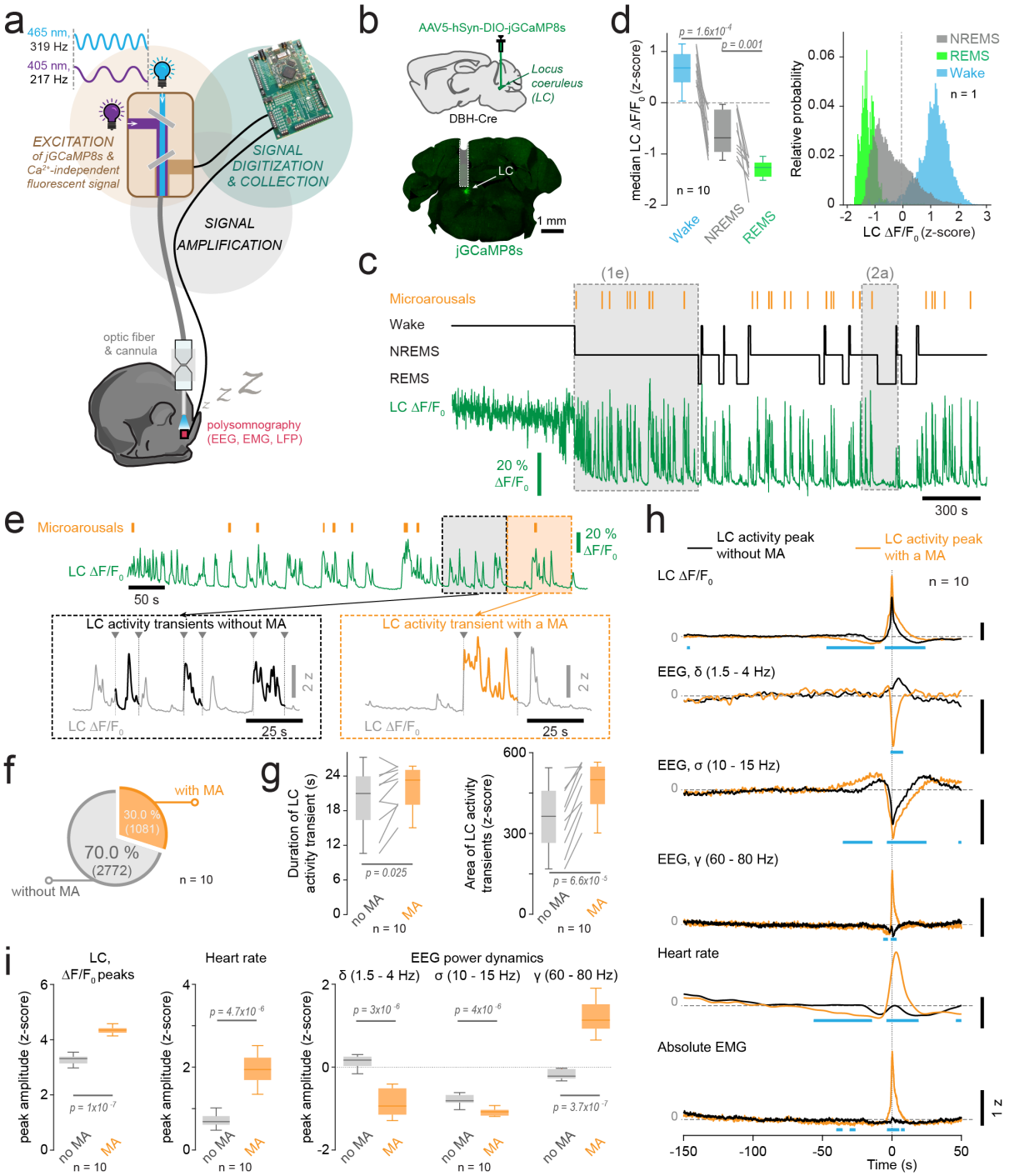

Figure 1. *Locus coeruleus* (LC) activity patterns across wakefulness, NREMS and REMS

a) Experimental scheme for sleep recordings in combination with fiber photometry.

b) Schematic of viral injection into a dopamine-β-hydroxylase (DBH)-Cre mouse prior to sleep/fiber photometric implantations and example *post hoc* histological verification of jGCaMP8s expression and optic fiber location.

c) Example sleep hypnogram (black) and jGCaMP8s fluorescent signal (green) recorded from LC (in $\Delta F/F_0$). Orange vertical lines: microarousals (MAs). Grey rectangles: trace portions that are expanded in other figure panels (as indicated).

d) Left, Box-and-whisker plot of mean LC fluorescence levels for wake, NREMS and REMS for Zeitgeber times (ZT) ZT0-ZT2 for n = 10 animals, with grey lines connecting values for individual animals; one-way repeated-measures ANOVA with *post hoc* t-tests. Bonferroni-corrected p = 0.025. Right, all-points-histogram for z-scored fluorescence across wake, NREMS and REMS for a representative animal.

e) Example trace expanded from panel c for NREMS. Orange vertical lines show MAs. Colored dotted rectangles indicate two trace portions expanded below. For these expanded portions, thick traces show LC activity transients without MAs (left) and with a MA (right). The on- and offset of these transients is marked with arrowheads connected to vertical lines. For further details, please see Extended Data Fig. 2.

f) Pie chart for proportion of LC activity transients without and with MAs in % for n = 10 animals for ZT0-ZT2. Numbers in parentheses include total counts of LC activity transients.

g) Box-and-whisker plots for duration (left) and area (right) of LC activity transients identified as illustrated in panel e for n = 10 animals. Grey lines connect mean values from individual animals.

h) Spectral analysis of EEG signals corresponding to LC activity peaks that were classified based on whether they occurred without a MA (black) or with a MA (orange). Corresponding power dynamics for the delta (δ), sigma (σ) and gamma (γ) frequency bands are aligned vertically, together with heart rate and absolute EMG. Traces denote means across n = 10 animals. Blue bars denote significance p values as calculated by false discovery rates.

i) Quantification of mean values from traces shown in h for peak values in the time interval 0-1s. All p values were calculated from paired *t*-tests. For power analyses, the Bonferroni-corrected p was 0.017.

See **Supplementary Table 1** for detailed statistical information.

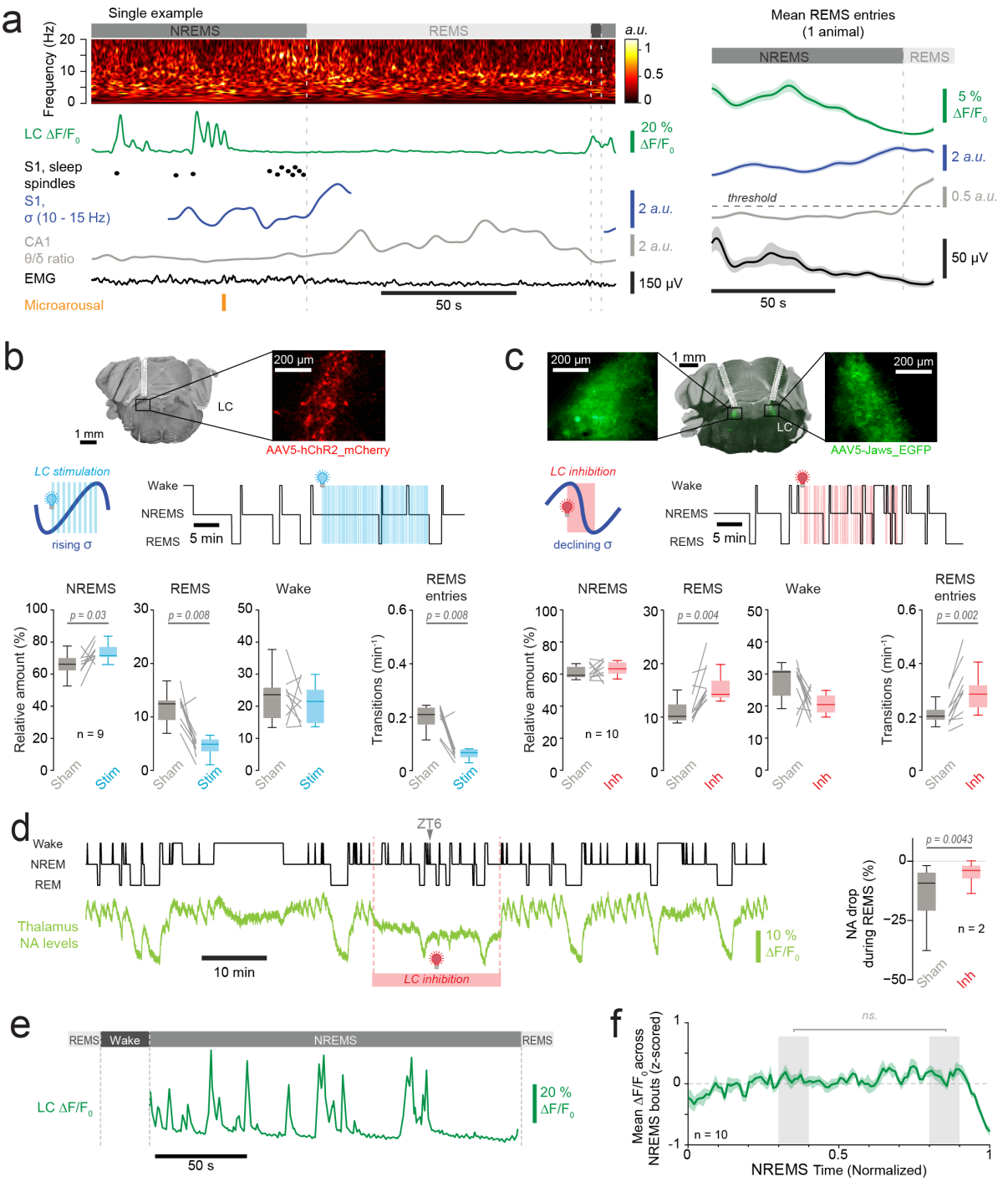

Figure 2. Association of LC activity patterns during NREMS with arousal promotion and REMS entries.

a) Left, Example recording of LC fluorescence during a NREMS-to-REMS transition ('REMS entry', expanded from Fig. 1c). Same signals shown as in a, with in addition CA1 θ/δ ratio and EMG. Right, Mean dynamics of these signals for the same animal.

b) Optogenetic stimulation of LC. Top, Histological verification of fiber positioning and viral transfection. Middle, Schematic of the light stimulation protocol based on closed-loop feedback analysis of σ power. Blue vertical lines show timing of optogenetic stimulation.

1005 Example portion of hypnogram is shown on the right. Bottom, Box-and-whisker-plot
1006 quantifications were calculated for the 20-min light *vs* sham (LED-off) stimulation periods for
1007 n = 9 animals. Grey lines, paired datasets per animal. Wilcoxon signed-rank tests.

1008 c) As a), for optogenetic inhibition of LC.

1009 d) Example dual fiber photometric recording from an animal that expressed Jaws in LC and
1010 $GRAB_{NE1h}$ in somatosensory thalamus. Portion underlain with orange square indicates period
1011 of LC inhibition. Quantification was done in n = 2 animals for 45 REMS bouts each in control
1012 and in light illumination. REMS bouts in both conditions were selected for equal durations
1013 before evaluating $GRAB_{NE1h}$ fluorescence decreases.

1014 e) Example trace for LC fluorescence during a NREMS bout.

1015 f) Mean LC fluorescence activity across time-normalized NREMS bouts. Shaded areas, data
1016 used for statistical analysis. Paired t-test.

1017 See **Supplementary Table 1** for detailed statistical information.

1018

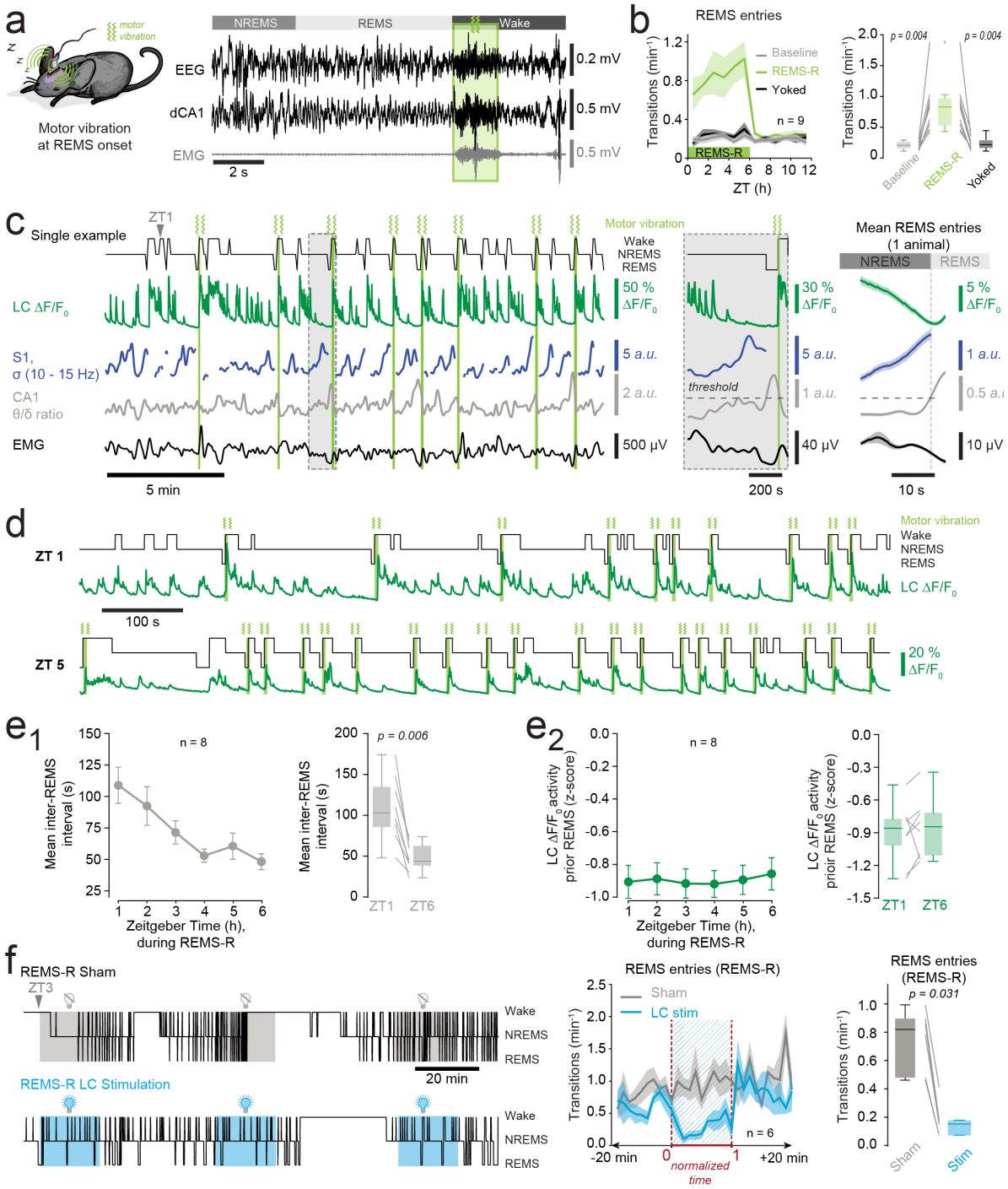

Figure 3. REMS restriction (REMS-R) unravels a minimal duration of the NREMS-REMS cycle related to LC activity decline.

a) Schematic of REMS-R implementation and representative recording showing (green rectangle with motor vibration symbol).

b) Frequency of REMS entries for n = 9 animals subjected to REMS-R from ZT0-ZT6, to yoked conditions (animals given vibrations timed to REMS from their neighbors) and to undisturbed conditions (baseline), followed by 6 h of recovery. To the right, box-and-whisker plot

1027 quantifications, with grey lines showing paired data for individual animals. Wilcoxon signed-
1028 rank test.
1029 c) Example recording during REMS-R, with grey rectangle indicating portion expanded on the
1030 right. Mean transitional dynamics calculated as in Fig. 2a.
1031 d) Example recording at ZT1 and at ZT5, corresponding to early and late moments during the
1032 REMS-R.
1033 e) e1) Quantification of mean (inter-REMS) intervals across a 6 h-REMS-R, with mean values
1034 shown on the right; e2) Same for LC activity levels in the 5 s before REMS entries. Grey lines
1035 connect paired data per animal. Paired t-tests for e1 and e2.
1036 f) Example recording for a REMS-R combined with Sham (LED-off) or optogenetic stimulation of
1037 LC at 1 Hz. Quantification of REMS entries across the stimulation period. Note the higher
1038 REMS transition frequency before optogenetic stimulation compared to baseline sleep (Fig. 2
1039 b, c). Box-and-whisker quantification of mean data for the entire REMS-R. Wilcoxon signed-
1040 rank test.
1041 See **Supplementary Table 1** for detailed statistical information.

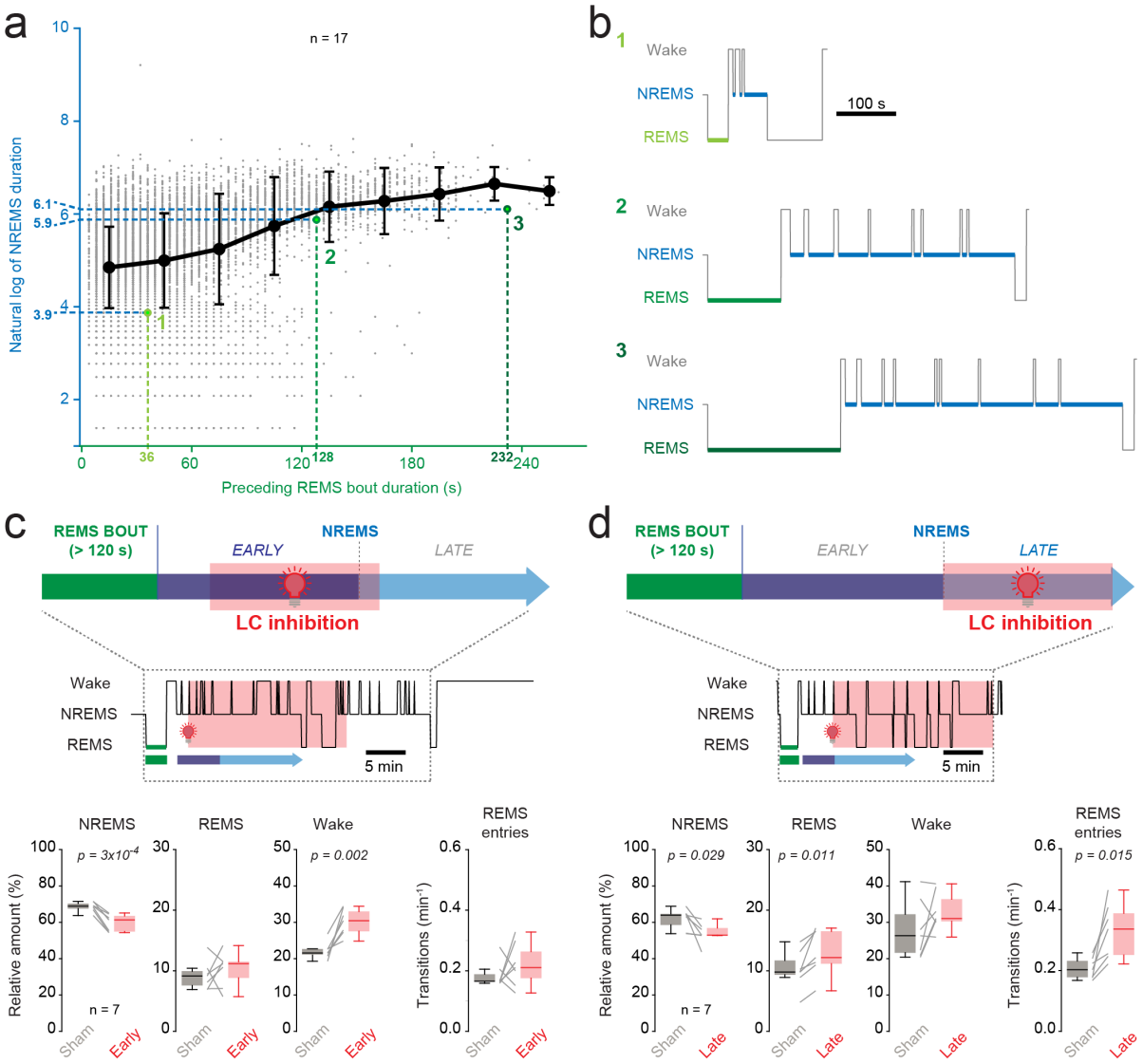

Figure 4. LC activity declines were necessary for REMS entries late but not early in the natural NREMS-REMS cycle.

a) Scatter plot of NREMS times (in units of natural logarithm) *vs* preceding REMS bout durations for undisturbed sleep of n = 17 animals in the light phase, as done in ref[44]. Datapoints marked by 1, 2 or 3 mark examples shown in panel b.

b) Representative examples for datapoints highlighted with numbers in panel a.

c) Top, schematic of the LC optogenetic inhibition protocol starting early in the NREMS bout once a REMS episode lasting > 120 s occurred. Example hypnogram is presented below. Box-and-whisker plots quantify times spent in wake, NREMS and REMS, and the frequency of REMS entries for early light inhibition (n = 7). Wilcoxon signed-rank or paired t-test.

d) As e, for LC inhibition starting late in the NREMS bout (n = 7). Wilcoxon signed-rank or paired t-tests.

See **Supplementary Table 1** for detailed statistical information.

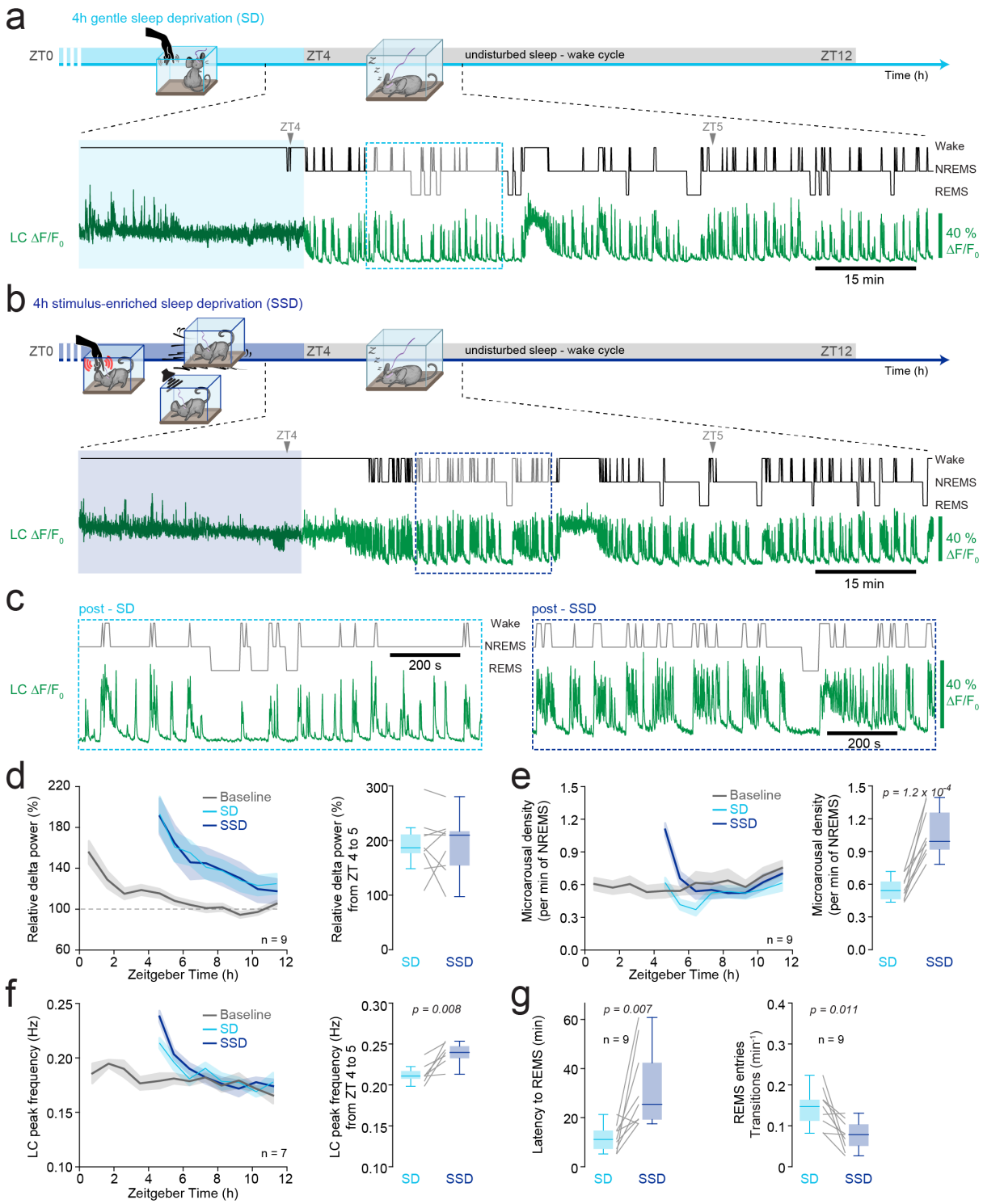

Figure 5. A stimulus-enriched but not a gentle sleep deprivation disrupted subsequent sleep and enhanced LC activity

a) Schematic of experimental timeline for gentle sleep deprivation (SD), with example hypnograms and corresponding LC fluorescence from the the end of the SD to 4 h in post-SD. Dotted rectangle indicates expanded portion in c.

1063 b) As a, for the stimulus-enriched sleep deprivation (SSD). Dotted rectangle indicates expanded
1064 portion in c.
1065 c) Expanded portions of traces in a, b.
1066 d) Mean dynamics of EEG δ power from ZT0-ZT12 for n = 9 animals subjected to baseline
1067 recordings, SD and SSD. Box-and-whisker quantification for data from ZT4-ZT5 on the right,
1068 corresponding to the first h after SD or SSD, with grey lines showing paired data per animal.
1069 Paired t-test.
1070 e) As c, for the density of MAs (n = 9). Paired t-test.
1071 f) As c, for LC peak frequency (n = 7). Paired t-test.
1072 g) Box-and-whisker quantification for REMS onset latency, quantified from the time of NREMS
1073 onset, and the transitions frequency of REMS entries, for the first h after SD or SSD (ZT4-ZT5,
1074 n = 9). Paired t-tests.
1075 See **Supplementary Table 1** for detailed statistical information.
1076
1077
1078
1079
1080
1081
1082
1083

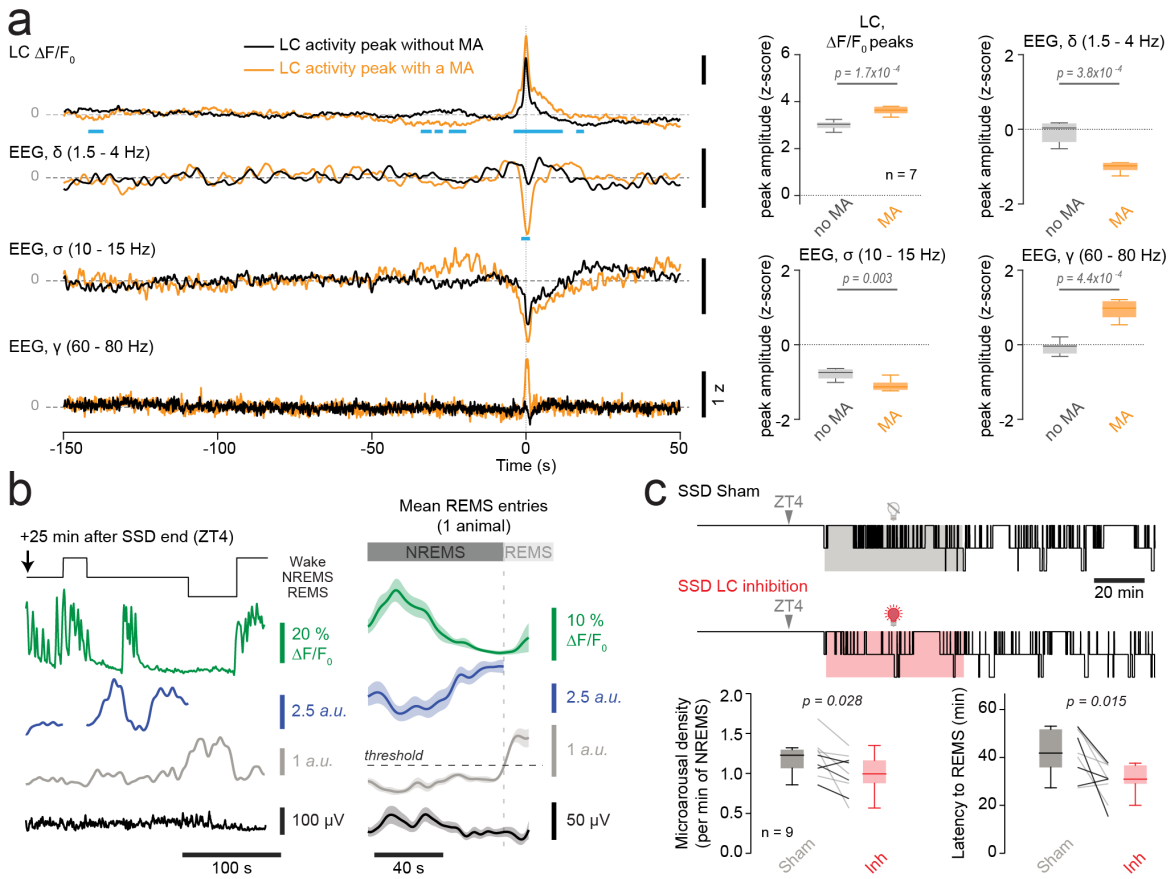

Figure 6. Acute LC inhibition suppressed sleep-disruptive effects of a stimulus-enriched wakefulness

a) Spectral analysis of EEG signals corresponding to LC activity peaks, as done in Fig. 1 h, I for the first 2 h after the end of the sensory stimulus-enriched sleep deprivation (SSD). LC activity peaks that are classified based on whether they occurred without a MA (black) or with a MA (orange). Traces denote means across n = 7 animals. Blue bars denote significance p values as calculated by false discovery rates. Quantification of mean values from traces shown in a for peak values for the time interval 0 – 1 s. All p values were calculated from paired *t*-tests. For power analyses, the Bonferroni-corrected p = 0.017.

b) Example recording of a REMS entry after SSD. Mean transitional dynamics calculated as in Fig. 2a.

c) Example hypnogram after SSD with or without Jaws-mediated optogenetic inhibition of LC. Box-and-whisker quantification of MA density and REMS onset latency after SSD with sham (LED-off) or light stimulation (n = 9). Grey and black lines connect data from animals exposed to 1-h or 2-h light-induced LC inhibition post-SSD. Paired *t*-test.

See **Supplementary Table 1** for detailed statistical information.

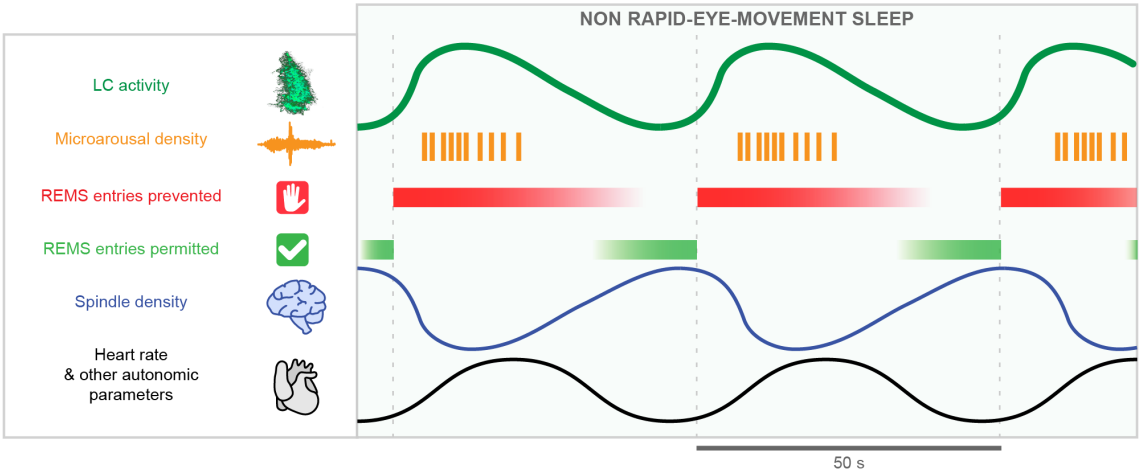

Figure 7. Scheme summarizing the functional partitioning of NREMS and its relevance for the NREMS-REMS cycle

From top to bottom, the time course of physiological parameters relevant for the partitioning of NREMS into arousability-promoting/REMS-supressing and REMS-promoting periods is illustrated. Two full cycles of this functional partitioning are shown, indicated by vertical dashed lines. Green thick lines: LC neuronal population Ca^{2+} activity; Orange: Frequency of MAs (see also ref [21]); Red and Green Stop and Go signals: REMS-suppressing and REMS-permissive periods; Blue line: Brain spectral fluctuations in sigma power (see also refs [17,22]); Black, Heart rate fluctuations (see also refs [17,22]). Other autonomic parameters include pupil size fluctuations as demonstrated in ref[72].